 doi:10.20944/preprints202110.0231.v1

Magnetic resonance imaging in animal models of Alzheimer's disease amyloidosis

Ruiqing Ni [1, 2*]

[1]Institute for Biomedical Engineering, ETH Zurich & University of Zurich, Zurich, Switzerland

[2]Institute for Regenerative Medicine, University of Zurich, Switzerland

* Correspondence:

Dr. Ruiqing Ni

ni@biomed.ee.ethz.ch

Keywords: Alzheimer's disease; amyloid-β; animal model; diffusion tensor imaging; functional imaging; magnetic resonance imaging; magnetic resonance spectroscopy;

 doi:10.20944/preprints202110.0231.v1

Abstract

Amyloid-beta (Aβ) plays an important role in the pathogenesis of Alzheimer's disease. Aberrant Aβ and tau accumulation induce neuroinflammation, cerebrovascular alterations, synaptic deficits, functional deficits, and neurodegeneration, leading to cognitive impairment. Animal models recapitulating the Aβ pathology such as transgenic, knock-in mouse and rat models have facilitated the understanding of disease mechanisms and development of therapeutics targeting at Aβ. There is a rapid advance in high-field MR in small animals. Versatile high-field magnetic resonance imaging (MRI) sequences such as diffusion tensor imaging, arterial spin labelling, resting-state functional MRI, anatomical MRI, MR spectroscopy as well as contrast agents have been developed for the applications in animal models. These tools have enabled high-resolution *in vivo* structural, functional, and molecular readouts with a whole brain field-of-view. MRI have been utilized to visualize non-invasively the Aβ deposits, synaptic deficits, regional brain atrophy, impairment in white matter integrity, functional connectivity, cerebrovascular and glymphatic system in animal models of amyloidosis. Many of the readouts are translational in clinical MRI in the brain of patients with Alzheimer's disease. In this review, we summarize the recent advance of using MRI for visualizing the pathophysiology in amyloidosis animal model. We discuss the outstanding challenges in brain imaging using MRI in small animal and propose future outlook in visualizing Aβ-related alterations in brain of animal models.

Preprints (www.preprints.org) | NOT PEER-REVIEWED | Posted: 15 October 2021 doi:10.20944/preprints202110.0231.v1

1. Introduction

The two core pathological hallmarks of Alzheimer's disease (AD) are extracellular amyloid-beta (Aβ) plaques and intracellular neurofibrillary tangles, resulting from the abnormal accumulation of misfolded Aβ and tau [1]. Aβ plays a central role in the pathogenesis of AD and downstream pathophysiological events [2]. The pathophysiological changes in AD start many years before the onset of clinical symptoms [3]. Recent advance in diagnostic imaging have provided insights into the time course of AD pathology, including Aβ, tau, neuroinflammation in patients and in animal disease models [4-6]. Magnetic resonance imaging (MRI) is widely used both in clinical setting for assisting the diagnosis towards precision medicine and in preclinical research in small animal models. Structural MRI for assessing the neurodegeneration (brain atrophy) in the ATN framework has offered valuable tool for early and differential diagnosis of AD and for disease staging [6,7]. Moreover multiplex MRI sequences such as diffusion tensor imaging (DTI) for white matter integrity assessment, resting-state (rs) functional MRI for functional connectivity [8], as well as arterial spin labelling (ASL) for cerebral perfusion have emerged as potential diagnostic biomarkers for AD.

Several generations of animal models of AD amyloidosis have been developed and facilitated the understanding of disease mechanisms and the development of treatment strategies. The models include transgenic APPswe, APP/PS1, APP23, J20 mice, and McGill-R-Thy1-APP rats [9-13], 2nd generation App^{NL-G-F}, App$^{hu/hu}$ knock-in and 3rd generation mouse models [14-17]. The animal models recapitulate the Aβ pathology and downstream gliosis, neuronal loss, functional and cognitive impairment. In addition, models haboring both Aβ and tau pathology such as 5×FAD, 3×Tg mice, and TgF344 rats have been widely used [18-20]. In this review, we summarize recent advances in MRI, contrast agents, and MR spectroscopy, fingerprinting in probing the alterations in brains of AD amyloidosis animal models. We outline the outstanding challenges and provide an outlook for further development of preclinical MR in animal models of AD amyloidosis.

2. Aβ imaging

The abnormal accumulation of Aβ deposits, both parenchymal plaques and cerebral amyloid angiopathy (CAA), particularly the neurotoxic oligomeric Aβ plays a crucial role in the disease pathogenesis in animal models and in patients with AD [2,21-23]. *In vivo* Aβ detection and longitudinal monitoring in mouse models of AD amyloidosis has provided insights on the disease mechanisms and treatment effects. The Aβ imaging at whole brain level have been mostly assessed

Preprints (www.preprints.org) | NOT PEER-REVIEWED | Posted: 15 October 2021 doi:10.20944/preprints202110.0231.v1

by using positron emission tomography (PET) for its excellent sensitivity [24,25]. Other imaging methods for *in vivo* Aβ detection such as two-photon microscopy, fluorescence molecular tomography and optoacoustic imaging assisted with specific probes have been developed [26-31]. MRI detection of Aβ deposits has also been developed with or without using contrast agents (**Table 1**). The advantage of MRI molecular imaging stem from its superior resolution compared to small animal PET. MRI without contrast agents have been developed by exploring high-resolution imaging and changes in tissue proton MR properties, such as T_2, T_2* [32,33] **(Figure 1e)**, magnetic susceptibility, magnetization transfer imaging [34,35] and chemical exchange-sensitive spin-lock (CESL) imaging [36]. T_2 relaxation time was found associated with Aβ pathology in several mouse models [37-39]. As iron, copper, zinc accumulate in the Aβ plaques [40,41], susceptibility weighted imaging (SWI) and quantitative susceptibility mapping (QSM) have been used to detect Aβ aggregates and iron accumulation in APP/PS1 and Tg-SwDI mice [42,43]. It is noted that the endogenous contrast-based (CE) MRI methods lack the sensitivity for Aβ plaque detection, thus generally requires a high magnetic field and long scan time.

A few exogenous MRI contrast agents that can specifically bind to Aβ have been developed, including 1) Gadolinium (Gd) based: Gd-diethylenetriamine pentaacetate (DTPA)-Aβ1-40, Gd-DTPA-K6Aβ1-30, cyanine-conjugated Gd (III) complex, Gd-pF(ab')24, liposomal macrocyclic Gd-ADx-001 [44-49] **(Figure 1f)**; 2) superparamagnetic iron oxide (SPIO) based: APP-SiMag, ultrasmall SPIO-polyethylene glycol-Aβ1-42.B, IgG4.1 NP bifunctional ultrasmall SPIO [50-54]. Dudeffant et al. demonstrated detection of compact Aβ plaques even around diameter of 25 μm as well as CAA and cerebral microhemorrhages in five mouse lines ($APP_{SL}/PS1_{M146L}$, $APP/PS1_{dE9}$, APP23, APP_{SwDI}, and 3×Tg) and in AD human brains using DOTAREM® (Gd-DOTA) at 7 T MRI [55]. The SPIO nanoparticles contrast require much smaller amount of injection compared due Gd-contrast agents due to the higher MR relaxivity. In addition, manganese (Mn) based, Mn oxide nanoparticles conjugated HMON-Aβ40 [37], Mn chloride [56], monocrystalline iron oxide nanoparticles [45], sialic acid coated bovine serum albumin magnetic nanoparticle [57] have been reported for Aβ deposits detection. 3) ^{19}F and ^{1}H MRI using contrast agents such as small chemical dye FSB, TFMB, bovine serum albumin@FDQDs, Shiga-Y5, and Shiga-Y51 have also been reported for *in vivo* Aβ imaging [47,58-62].

Preprints (www.preprints.org) | NOT PEER-REVIEWED | Posted: 15 October 2021 doi:10.20944/preprints202110.0231.v1

Moreover, several contrast agents specific for Aβ oligomer (antibody based or chemical probe) have been reported. Viola et al. reported using 12-16 nm Fe_3O_4 magnetic nanostructures (MNS) conjugated with Aβ oligomer specific antibody NU4 for detecting Aβ oligomers in the mouse brains [63]. Rozema et al. reported Aβ oligomer specific antibody based ACU193-MNS for detecting the Aβ oligomer level in rabbit by using MRI [64]. As the size of antibody hinders its blood-brain barrier (BBB) permeability, one strategy is to facilitate its delivery is to link a fraction of antibody with transferrin [65] or scavenger receptor. Liu et al. developed W20/XD4-SPIO nanoparticles, which are multifunctional SPIO nanoparticles conjugated with Aβ oligomer-specific single-chain variable fragment (scFv) of the antibody and scavenger receptor, and demonstrated the *in vivo* detection in APP/PS1 mice [66] (**Figure 1g-h**). Chen et al. and Dong et al. reported curcumin derivative conjugated magnetic nanoparticle Cur-MNPs for *in vivo* imaging of Aβ with high contrast in APPswe and 5×FAD mice [67,68].

3. Functional imaging

Synaptic impairment, aberrant excitatory neuronal activity, gamma oscillations and disrupted circuit are early features in amyloidosis animal models [69-72]. Clusters of hyperactive neurons are observed in the vicinity of Aβ plaques in APP mouse models [73]. There is a vicious cycle of Aβ-dependent neuronal hyperactivation initiated by suppression of glutamate reuptake [74]. Neurovascular uncoupling and impaired cerebral blood flow (CBF) have been demonstrated by MRI and optical imaging modalities [75].

3.1 Magnesium enhanceed (ME) MRI

Both neuronal tracing MEMRI and the activity-induced MEMRI method for detecting active neural regions during a task or stimulation, independent of hemodynamics have been developed [76,77]. However the dose of Mn chloride required in *in vivo* imaging study might lead to increased risk of acute toxicity in the liver, heart, and kidney, therefore is not widely applied (90). Activity-induced MEMRI have been applied in APPswe, APP×PS1-Ki, CVN-AD, J20, 5×FAD mice and TgF344 rats [56,78-81] (**Table 2**). Most MEMRI studies found hyperactivation and functional abnormalities in the APP animal models. Although studies also reported that the activity-induced MEMRI cannot detect hyperactivation in the APP×PS1-Ki [78]. MEMRI study in TetO/APP_{SwInd} with overexpression of APP specifically in olfactory neurons was shown to detect laminar changes and neurodegeneration in the olfactory bulb [82]. Yoshikawa et al. showed that tau depletion in APP transgenic mice reduced

Preprints (www.preprints.org) | NOT PEER-REVIEWED | Posted: 15 October 2021 doi:10.20944/preprints202110.0231.v1

the task-related hippocampal hyperactivation by using MEMRI and the spatial memory impairment [79]. Neuronal Tracing Studies With MEMRI by direct injection of Mn into mouse brain region can detect impaired axon transport. Thus, MEMRI can be used to study axonal transport and measure axonal transport rates in the rodent brain. Intranasal administration of manganese showed decreased axonal transport rates in olfactory system prior to Ab plaque formation in mouse model in APPswe and 3×Tg mice [83-85], and in the hippocampus-basal forebrain pathway in TetO/APP_{SwInd} mice [86].

3.2 Resting state-fMRI

fMRI has enabled a better understanding on brain activity in different areas and has become a workhorse in neuroimaging [8], and potential early biomarker for neurodegenerative diseases. Blood-oxygen-level-dependent (BOLD) signal from rs-fMRI has been widely used as a readout for brain function [87]. The fMRI in small animal model is more challenging compared to human brain imaging, due to their dependence on multiple factors such as fluctuations, spatial localization, nonlinearities, baseline physiological state, pulse sequence and task [88,89]. Early hypersynchrony of BOLD resting-state networks in the telencephalic, interhemispheric, hippocampal regions as well as fornix has been reported in APP mouse models, providing predictive value for the later cognitive dysfunction [81,90-97] **(Table 2)**. Latif-Hernandez et al. reported that subtle behavioral changes and increased prefrontal-hippocampal network synchronicity in APP^{NL-G-F} mice before prominent plaque deposition [98]. Ben-Nejma et al. reported increased soluble Aβ causes early aberrant brain network hyper-synchronisation in the default mode network (DMN)-like brain regions at 8 weeks post doxycycline treatment in inducible transgenic Tet-Off APP animal model; And hypo-synchronization was detected by fMRI at 20 week post doxycycline treatment in a mature-onset Tet-Off APP mice [99](**Figure 1a-d**). Other study reported diminished functional connectivity in APP/PS1 mice [100]. Early hyperactivation have been reported also in the animal models haboring both Aβ and tau pathology; Gail Canter et al. demonstrated that the DMN was affected early at 4 month-of-age and the limbic system at 6 month-of-age along with a network-specific amyloid progression in 5×FAD mice [101]. Tudela et al. reported an early alteration in the anterior DMN subnetwork of TgF344 rats compared to controls by rs-fMRI using independent component analysis [102].

3.3 ASL

Preprints (www.preprints.org) | NOT PEER-REVIEWED | Posted: 15 October 2021 doi:10.20944/preprints202110.0231.v1

ASL is a MRI technique to quantify tissue blood flow or perfusion, which is routinely performed in the clinical setting [103]. Cortical hypoperfusion by using ASL have been reported in APP/PS1, Tg-SwDI, arcAβ, APPswe, APP23 mice [33,104-112] as well as in 3×Tg, bigenic and 5×FAD mice harboring both Aβ and tauopathy (**Table 2**) **(Figure 1f)**. Reduced cortical CBF was observed in the aged arcAβ mouse (24 month-of-age) compared to aged wild-type mice and compared to young arcAβ **(Figure 2i, j**). Recent study by Cruz Hernández et al. demonstrated that neutrophil adhesion in brain capillaries impaired the CBF and that treatment using anti-neutrophil marker antibody reversed the CBF reduction and improved the impaired memory function in APP/PS1 mice [104]. In addition to ASL, several new MR perfusion method have been developed.

3.4 Cerebrovascular reactivity measurement

Vasodilatory stimulus challenged fMRI assesses the cerebrovascular reactivity based on the cerebral haemodynamic changes, and reflects the vascular reserve and autoregulatory function [113]. Different vasodilatory stimulus including carbon-dioxide, breath-hold task (in human), and acetazolamide have been used [114,115]. Impaired cerebrovascular reactivity by using fMRI with carbon-dioxide as the stimulus has been reported in patients with mild cognitive impairment and AD [113,116,117]. In AD mouse model, Gd or SPIO based contrast agent (e.g. Endorem) was intravenous injected to monitor the signal alterations due to administration of acetazolamide [114]. A reduced cerebrovascular reactivity has been reported in a few APP mouse models including APP/PS1, arcAβ, APPswe, APP23, J20, PDAPP, and BiAT mice [53,107,118-120]**(Table 2).**

4 Neurochemical changes detection

4.1 MRS

MRS has been shown detecting the distinct metabolic profiles in APP/PS1 mice [121-126], J20 mice [109], APPswe mice [127,128] compared to wild-type mice respectively. Several studies have reported reduced N-acetylaspartate /creatine ratio [125] and [124], lower glutamate levels [123] in APP/PS1 mice compared to wild-type mice. In animal models haboring both Aβ and tau pathology, including 3×Tg [129], 5×FAD mice [130], APP/PS2/Tau mice [131] and TgF344 rat [132] **(Table 2)**. Lee et al.

Preprints (www.preprints.org) | NOT PEER-REVIEWED | Posted: 15 October 2021 doi:10.20944/preprints202110.0231.v1

demonstrated a 35 % decrease in the availability of metabotropic glutamate receptor 5 measured by PET and a decrease in glutamate, N-acetylaspartate and taurine, levels and an increase in lactate level by ^{1}H MRS in 5×FAD mice compared to wild-type at 5 months-of-age [130]. Chiquita et al. showed an early hippocampal taurine loss by longitudinal MRS in 3×Tg mice [129]. Micotti et al. reported striatal atrophy and increases in the levels of myo-inositol in TASTPM and APP/PS2/Tau mice compared to wild-type mice, respectively [131].

4.2 Chemical exchange saturation transfer (CEST)

Molecular MR imaging based on CEST offers improved sensitivity, and can detect changes of glucose, glutamate, creatine, and myoinositol. Glucose CEST MRI is a recently developed technique that detects unlabeled glucose at physiologically relevant concentrations using proton-only MRI scanners (Table 2). Tolomeo et al. demonstrated glucose CEST detection of reduced cerebral 2-deoxy-D-glucose uptake in APP23 mice compared to wild-type mice [133]. Using dynamic glucose-enhanced MRI, Huang et al. demonstrated an altered level of D-glucose in brain parenchymal as well as in the cerebrospinal fluid (CSF) of aged APP/PS1 mice compared to wild-type mice [134]. Igarashi et al. demonstrated a reduced level of glutamate as an indicator of synaptic dysfunction measured by using glutamate CEST in the parietal cortex, but not in the hippocampus of 5×FAD mice [135]. Chen et al. demonstrated that creatine CEST detection of creatine level were reduced in the cortex and corpus callosum of APP/PS1 mice compared to wild-type mice at 6 months-of-age [136]. Chen et al. showed that reduced saturation transfer difference for the composite protein amide proton in APP/PS1 mice at compared to the age-matched wild-type mice [137].

5 Cerebrovascular imaging

Accumulating evidence indicates the vascular contribution to cognitive impairment and dementia in AD [138,139]. Impaired cerebral vasculature were reported in various amyloidosis amyloid model with parenchymal Aβ plaques and different level of CAA [140-142].

5.1 SWI

Preprints (www.preprints.org) | NOT PEER-REVIEWED | Posted: 15 October 2021 doi:10.20944/preprints202110.0231.v1

The presence of iron can be detected by MRI due to its effect on the surrounding tissue, giving rise to detectable changes in transverse T_2 relaxation by using T_2* and susceptibility by using SWI and QSM (**Table 3**). Previous X ray microscopy study reported that particulate and crystalline iron was detected inside the dense plaque core in the APP/PS1 mouse brain accumulation is associated with Aβ plaque [143]. Beckmann et al. showed microhemorrhages in β-secretase inhibitor treated APP23 mice by using T_2* weighted imaging [144]. Recent study by Maniskas et al. demonstrated a gender differences in the number of cerebral microbleeds by T_2* sequence in Tg-SwDI mice (higher load in female) [145]. SWI and QSM have been performed in arcAβ, APP/PS1 and CVN-AD mice at 9.4 T [81,146-149]. McIntosh et al, showed that iron accumulation detected by SWI contributed to altered cerebral metabolism and cognitive impairment observed in APP/PS1 mice [148].

5.2 MR Angiography (MRA)

(MRA has been widely used in clinical setting and in the small animal imaging for assessing the cerebrovasculature abnormalities. Intracranial stenosis assessed by using MRA was observed in patients with cognitive impairment and AD [150,151]. Both time-of-flight MRA and CE MRA have been applied in amyloidosis animal models (**Table 3**). Detection of vascular alterations by *in vivo* MRA and histology has been reported in APP/PS1, arcAβ, APP/PS1, APP23 mice [39,118,128,152,153]. Klohs et al. demonstrated and reduced density and remodeling of cerebral microvasculature by using CE MRA reveals in aged arcAβ mice [152](**Figure 2e-h**). MR Q mapping assisted with SPIO further showed a reduced microvessel density, correlating with the levels of Aβ pathology in the brain of arcAβ mice [154]. In addition to MRA, several recent MR techniques have been developed for assessing the cerebrovasculature and applied in AD animal models. Chang et al reported using diffusion weighted imaging and monocrystalline iron oxide nanoparticle for vessel size index, diameter, density, mean vessel-weighted image and blood volume fraction in 5×FAD mice [155]. Leaston et al. showed early vascular abnormalities in APOE4 knock in rats compared to wild-type rats by using quantitative ultra-short time-to-echo (QUTE) CE-MRI [156]. MR elastography have been applied and detected impaired cerebral viscoelastic properties by using in 5×FAD, APP/PS1 and APP23 mice [157-159]. Montagne et al demonstrated T_2*weighted imaging of brain cerebrovascular inflammation assisted with micro-sized particles of iron oxide (MPIO) targeting vascular cell adhesion molecule 1 (VCAM-1), MPIOaVCAM-1, in APP/PS1 mice [160].

Preprints (www.preprints.org) | NOT PEER-REVIEWED | Posted: 15 October 2021 doi:10.20944/preprints202110.0231.v1

6 Structural imaging

6.1 Volumetric imaging for brain atrophy

In vivo MRI using T_1 and T_2 scans and histological evaluation have identified differences in whole or regional brain volumes between amyloidosis and wild-type animal models, including APP T714I, APP/PS1, APP/PS1 KI, 3×Tg, TASTPM mice and McGill-R-Thy1-APP rats [127,161-168] **(Table 3).** Delatour et al. reported global atrophy, enlarged CSF space in the posterior brain areas, and midbrain area in fiber tracts in APP/PS1 mice compared to wild-type mice [168]. Badhwar et al. demonstrated that there is an impaired spatial learning/memory-induced volume increase in the hippocampus in APP/J20 mice compared to wild-type mice [169]. However conflicting observations of no general pathological brain atrophy have also been reported in aged APP/PS1 mice [164].

6.2 DTI

Extensive myelin loss was observed in APP mice and in individuals with AD both by *in vivo* imaging as well as in histopathological studies **[170-172]**. Recent studies showed that myelin loss drives Aβ deposition, and that enhancing myelin renewal in turn alleviate the cognitive deficits in APP/PS1 mice **[173]** and in 5×FAD mice **[174]**. A number of studies have applied *in vivo* and *ex vivo* DTI for detecting the white matter impairment, which appears preceding the anatomical changes on structural MRI including the APPswe, APP/PS1, TgCRND8, APP^{NL-G-F}, 3×Tg, CVN-AD and 5×FAD mice **[81,93,97,175-183]** (**Table 3**). In addition to DTI, diffusion kurtosis imaging (DKI) and quantitative magnetization transfer imaging (qMTI) have been applied in APP mouse models where hippocampal alterations were observed **[178,184]**. However the observed DTI scalars are not consistent across different studies, probably due to the dynamic microstructural changes various animal models **[94,185]**. Reduced fractional anisotropy (FA), and both reduced/increased radial diffusivity (RD) were reported in aged APPswe mice **[175,186,187]**. Falangola et al. and Zhou et al. reported basal forebrain cholinergic abnormalities detected by DTI and DKI in in 3×Tg mice **[188,189]**, while Kastyak-Ibrahim et al. reported lack of white matter pathology in the same mouse line **[190]**. The white matter impairment has been found associated with microglia activation in the CVN-AD mice **[97]**. In addition, reduced FA also been reported in gray matter in the brain of 3×Tg, APP/PS1 and APP23 mice **[93,123,171,177,186,191,192]**. Colon-Perez et al imaged the TgCRND8 mice *in vivo* using diffusion MRI at 11.1 T and calculated using neurite orientation dispersion and density imaging (NODDI)

Preprints (www.preprints.org) | NOT PEER-REVIEWED | Posted: 15 October 2021 doi:10.20944/preprints202110.0231.v1

model [193]: reduced FA, RD, and increased orientation dispersion and intracellular volume fraction were detected in the white matter and the hippocampus.

7. Discussion

With the increased availability and technological development in small animal MRI, there is a rapid advance in application in AD amyloidosis animal models in the recent years in molecular, functional and structural imaging. Here we propose several remaining knowledge gaps in MR imaging in AD amyloidosis animal models that has not been fully established or investigated:

BBB integrity imaging: BBB impairment plays an important role in AD pathogenesis, neural dysfunction and is associated with cognitive decline [194-199]. However, conflicting data showing lack of widespread BBB leakage has also been reported in several AD animal models [200]. Dynamic contrast-enhanced (DCE)-MRI have been utilized to show the impaired BBB integrity in the hippocampus of patients of early AD [201]. So far, very few studies have visualized the BBB integrity by using MRI in animal models of AD. Montagne et al. recently showed an impaired BBB integrity by using DCE-MRI assisted with Gd-DTPA in 5×FAD and *APOE4* mice [202] (**Figure 2a-d**) (**Table 3**). Dickie et al. reported that DCE-MRI did not detected the difference between the TgF344 and wild-type rats at 18 months-of-age, and that increased BBB water permeability was detected by using multi-flip angle multi-echo (MFAME) water-exchange MRI in TgF344 rats compared to wild-type [203]. Using the same method, Dickie et al. further showed in a cross-sectional study that BBB water permeability is affected earlier in TgF344 rats (between 13-18 months-of-age) compared to that in wild-type mice in normal ageing (between 18-21 months-of-age) [204]. Further studies are required to further establish non-invasive imaging tools for visualizing BBB integrity and to elucidate the degree and role of BBB impairment in AD animal models.

Glymphatic system imaging: The glymphatic system has been shown important for the exchange of CSF with interstitial fluid, and for clearance of the waste metabolites involving the aquaporin 4 water channel [205]. Emerging evidence suggests that the glymphatic system dysfunction may contribute to the development of AD [205-208]. Recent studies by Da Mesquita et al. also showed impaired meningeal lymphatics in J20 and 5×FAD mice, affecting microglia responses and the effect of anti-Aβ immunotherapy [209,210]. DCE-MRI using Gd-contrast agents have been developed to examine the brain-wide glymphatic system in both healthy and diseased brains in human [211,212] in mice and

rats [213-217]. Harrison et al recently showed an reduced clearance of tau in rTg4510 mice of 4-repeat tauopathy compared to wild-type mice by DCE-MRI using Gd-DTPA [213]. In addition to DCE-MRI, DTI analysis along the perivascular space [218], phase alternate labelling with null recovery MRI [219], and Mn^{2+} nanoconstruct for MRI detection of CSF [220] are being developed for studying the interstitial and CSF flow kinetics. *In vivo* MR imaging for the glymphatic system in amyloidosis animal models remains to be demonstrated.

In summary, the multiplex non-invasive MRI have significantly improved our understanding of the pathophysiology in the AD amyloid animal models at a systematic level and provided possibility for longitudinal monitoring of disease development.

Declaration of Interest

The authors declare no completing interest relevant to the submitted manuscript.

Author Contributions

RN wrote the manuscript and approved the submission of the manuscript.

Funding

RN received funding from Helmut Horten Stiftung, Vontobel Stiftung, and UZH Entrepreneur Fellowship of the University of Zurich, reference no. [MEDEF-20-021].

References

1. Scheltens, P.; De Strooper, B.; Kivipelto, M.; Holstege, H.; Chételat, G.; Teunissen, C.E.; Cummings, J.; van der Flier, W.M. Alzheimer's disease. *The Lancet* **2021**, *397*, 1577-1590, doi:10.1016/S0140-6736(20)32205-4.
2. Haass, C.; Selkoe, D.J. Soluble protein oligomers in neurodegeneration: lessons from the Alzheimer's amyloid beta-peptide. *Nat Rev Mol Cell Biol* **2007**, *8*, 101-112, doi:10.1038/nrm2101.
3. Jack, C.R., Jr.; Bennett, D.A.; Blennow, K.; Carrillo, M.C.; Dunn, B.; Haeberlein, S.B.; Holtzman, D.M.; Jagust, W.; Jessen, F.; Karlawish, J.; et al. NIA-AA Research Framework: Toward a biological definition of Alzheimer's disease. *Alzheimers Dement* **2018**, *14*, 535-562, doi:10.1016/j.jalz.2018.02.018.

4. Villemagne, V.L.; Dore, V.; Burnham, S.C.; Masters, C.L.; Rowe, C.C. Imaging tau and amyloid-beta proteinopathies in Alzheimer disease and other conditions. *Nat Rev Neurol* **2018**, *14*, 225-236, doi:10.1038/nrneurol.2018.9.

5. Leng, F.; Edison, P. Neuroinflammation and microglial activation in Alzheimer disease: where do we go from here? *Nature Reviews Neurology* **2021**, *17*, 157-172, doi:10.1038/s41582-020-00435-y.

6. Dubois, B.; Villain, N.; Frisoni, G.B.; Rabinovici, G.D.; Sabbagh, M.; Cappa, S.; Bejanin, A.; Bombois, S.; Epelbaum, S.; Teichmann, M.; et al. Clinical diagnosis of Alzheimer's disease: recommendations of the International Working Group. *The Lancet Neurology* **2021**, *20*, 484-496, doi:https://doi.org/10.1016/S1474-4422(21)00066-1.

7. Frisoni, G.B.; Fox, N.C.; Jack, C.R., Jr.; Scheltens, P.; Thompson, P.M. The clinical use of structural MRI in Alzheimer disease. *Nature reviews. Neurology* **2010**, *6*, 67-77, doi:10.1038/nrneurol.2009.215.

8. Fox, M.D.; Raichle, M.E. Spontaneous fluctuations in brain activity observed with functional magnetic resonance imaging. *Nat Rev Neurosci* **2007**, *8*, 700-711, doi:10.1038/nrn2201.

9. Radde, R.; Bolmont, T.; Kaeser, S.A.; Coomaraswamy, J.; Lindau, D.; Stoltze, L.; Calhoun, M.E.; Jaggi, F.; Wolburg, H.; Gengler, S.; et al. Abeta42-driven cerebral amyloidosis in transgenic mice reveals early and robust pathology. *EMBO Rep* **2006**, *7*, 940-946, doi:10.1038/sj.embor.7400784.

10. Hsiao, K.; Chapman, P.; Nilsen, S.; Eckman, C.; Harigaya, Y.; Younkin, S.; Yang, F.; Cole, G. Correlative memory deficits, Abeta elevation, and amyloid plaques in transgenic mice. *Science* **1996**, *274*, 99-102, doi:10.1126/science.274.5284.99.

11. Mucke, L.; Masliah, E.; Yu, G.Q.; Mallory, M.; Rockenstein, E.M.; Tatsuno, G.; Hu, K.; Kholodenko, D.; Johnson-Wood, K.; McConlogue, L. High-level neuronal expression of abeta 1-42 in wild-type human amyloid protein precursor transgenic mice: synaptotoxicity without plaque formation. *J Neurosci* **2000**, *20*, 4050-4058, doi:10.1523/jneurosci.20-11-04050.2000.

12. Richards, J.G.; Higgins, G.A.; Ouagazzal, A.M.; Ozmen, L.; Kew, J.N.; Bohrmann, B.; Malherbe, P.; Brockhaus, M.; Loetscher, H.; Czech, C.; et al. PS2APP transgenic mice, coexpressing hPS2mut and hAPPswe, show age-related cognitive deficits associated with discrete brain amyloid deposition and inflammation. *J Neurosci* **2003**, *23*, 8989-9003, doi:10.1523/jneurosci.23-26-08989.2003.

13. Sturchler-Pierrat, C.; Abramowski, D.; Duke, M.; Wiederhold, K.H.; Mistl, C.; Rothacher, S.; Ledermann, B.; Bürki, K.; Frey, P.; Paganetti, P.A.; et al. Two amyloid precursor protein transgenic mouse models with Alzheimer disease-like pathology. *Proc Natl Acad Sci U S A* **1997**, *94*, 13287-13292, doi:10.1073/pnas.94.24.13287.

14. Saito, T.; Matsuba, Y.; Mihira, N.; Takano, J.; Nilsson, P.; Itohara, S.; Iwata, N.; Saido, T.C. Single App knock-in mouse models of Alzheimer's disease. *Nat Neurosci* **2014**, *17*, 661-663, doi:10.1038/nn.3697.

15. Serneels, L.; T'Syen, D.; Perez-Benito, L.; Theys, T.; Holt, M.G.; De Strooper, B. Modeling the β-secretase cleavage site and humanizing amyloid-beta precursor protein in rat and mouse to study Alzheimer's disease. *Molecular Neurodegeneration* **2020**, *15*, 60, doi:10.1186/s13024-020-00399-z.

16. Sato, K.; Watamura, N.; Fujioka, R.; Mihira, N.; Sekiguchi, M.; Nagata, K.; Ohshima, T.; Saito, T.; Saido, T.C.; Sasaguri, H. A 3(rd) generation mouse model of Alzheimer's disease shows early and increased cored plaque pathology composed of wild-type human amyloid β peptide. *J Biol Chem* **2021**, 101004, doi:10.1016/j.jbc.2021.101004.

17. Baglietto-Vargas, D.; Forner, S.; Cai, L.; Martini, A.C.; Trujillo-Estrada, L.; Swarup, V.; Nguyen, M.M.T.; Do Huynh, K.; Javonillo, D.I.; Tran, K.M.; et al. Generation of a humanized Aβ expressing mouse demonstrating aspects of Alzheimer's disease-like pathology. *Nature Communications* **2021**, *12*, 2421, doi:10.1038/s41467-021-22624-z.

18. Oakley, H.; Cole, S.L.; Logan, S.; Maus, E.; Shao, P.; Craft, J.; Guillozet-Bongaarts, A.; Ohno, M.; Disterhoft, J.; Van Eldik, L.; et al. Intraneuronal beta-amyloid aggregates, neurodegeneration, and neuron loss in transgenic mice with five familial Alzheimer's disease mutations: potential factors in amyloid plaque formation. *J Neurosci* **2006**, *26*, 10129-10140, doi:10.1523/jneurosci.1202-06.2006.

19. Oddo, S.; Caccamo, A.; Shepherd, J.D.; Murphy, M.P.; Golde, T.E.; Kayed, R.; Metherate, R.; Mattson, M.P.; Akbari, Y.; LaFerla, F.M. Triple-transgenic model of Alzheimer's disease with plaques and tangles: intracellular Abeta and synaptic dysfunction. *Neuron* **2003**, *39*, 409-421, doi:10.1016/s0896-6273(03)00434-3.

20. Cohen, R.M.; Rezai-Zadeh, K.; Weitz, T.M.; Rentsendorj, A.; Gate, D.; Spivak, I.; Bholat, Y.; Vasilevko, V.; Glabe, C.G.; Breunig, J.J.; et al. A transgenic Alzheimer rat with plaques, tau pathology, behavioral impairment, oligomeric aβ, and frank neuronal loss. *J Neurosci* **2013**, *33*, 6245-6256, doi:10.1523/jneurosci.3672-12.2013.

21. Lesné, S.; Koh, M.T.; Kotilinek, L.; Kayed, R.; Glabe, C.G.; Yang, A.; Gallagher, M.; Ashe, K.H. A specific amyloid-β protein assembly in the brain impairs memory. *Nature* **2006**, *440*, 352-357, doi:10.1038/nature04533.

22. Lambert, M.P.; Velasco, P.T.; Chang, L.; Viola, K.L.; Fernandez, S.; Lacor, P.N.; Khuon, D.; Gong, Y.; Bigio, E.H.; Shaw, P.; et al. Monoclonal antibodies that target pathological assemblies of Aβ. *J. Neurochem.* **2007**, *100*, 23-35, doi:10.1111/j.1471-4159.2006.04157.x.

23. Shankar, G.M.; Li, S.; Mehta, T.H.; Garcia-Munoz, A.; Shepardson, N.E.; Smith, I.; Brett, F.M.; Farrell, M.A.; Rowan, M.J.; Lemere, C.A.; et al. Amyloid-β protein dimers isolated directly from Alzheimer's brains impair synaptic plasticity and memory. *Nat Med* **2008**, *14*, 837-842, doi:10.1038/nm1782.

24. Snellman, A.; Rokka, J.; Lopez-Picon, F.R.; Helin, S.; Re, F.; Loyttyniemi, E.; Pihlaja, R.; Forloni, G.; Salmona, M.; Masserini, M.; et al. Applicability of [(11)C]PIB micro-PET imaging for in vivo follow-up of anti-amyloid treatment effects in APP23 mouse model. *Neurobiol Aging* **2017**, *57*, 84-94, doi:10.1016/j.neurobiolaging.2017.05.008.

25. Rodriguez-Vieitez, E.; Ni, R.; Gulyas, B.; Toth, M.; Haggkvist, J.; Halldin, C.; Voytenko, L.; Marutle, A.; Nordberg, A. Astrocytosis precedes amyloid plaque deposition in Alzheimer APPswe transgenic mouse brain: a correlative positron emission tomography and in vitro imaging study. *European journal of nuclear medicine and molecular imaging* **2015**, *42*, 1119-1132 doi:10.1007/s00259-015-3047-0.

26. Polatoglu, M.N.; Liu, Y.; Ni, R.; Ripoll, J.; Rudin, M.; Wolf, M.; Ren, W. Simulation of Fluorescence Molecular Tomography using a Registered Digital Mouse Atlas. In Proceedings of the Clinical and Preclinical Optical Diagnostics II, Munich, 2019/06/23, 2019; p. 11074_11011.

27. Ni, R.; Villois, A.; Dean-Ben, X.L.; Chen, Z.; Vaas, M.; Stavrakis, S.; Shi, G.; deMello, A.; Ran, C.; Razansky, D.; et al. In-vitro and in-vivo characterization of CRANAD-2 for multi-spectral optoacoustic tomography and fluorescence imaging of amyloid-beta deposits in Alzheimer mice. *Photoacoustics* **2021**, *23*, 100285, doi:https://doi.org/10.1016/j.pacs.2021.100285.

28. Calvo-Rodriguez, M.; Hou, S.S.; Snyder, A.C.; Dujardin, S.; Shirani, H.; Nilsson, K.P.R.; Bacskai, B.J. In vivo detection of tau fibrils and amyloid β aggregates with luminescent conjugated oligothiophenes and multiphoton microscopy. *Acta Neuropathologica Communications* **2019**, *7*, 171, doi:10.1186/s40478-019-0832-1.

29. Ni, R.; Chen, Z.; Shi, G.; Villois, A.; Zhou, Q.; Arosio, P.; Nitsch, R.M.; Nilsson, K.P.R.; Klohs, J.; Razansky, D. Transcranial in vivo detection of amyloid-beta at single plaque resolution with large-field multifocal illumination fluorescence microscopy. *bioRxiv* **2020**, 2020.2002.2001.929844, doi:10.1101/2020.02.01.929844.

30. Ni, R.; Dean-Ben, X.L.; Kirschenbaum, D.; Rudin, M.; Chen, Z.; Crimi, A.; Voigt, F.F.; Nilsson, K.P.R.; Helmchen, F.; Nitsch, R. Whole brain optoacoustic tomography reveals strain-specific regional beta-amyloid densities in Alzheimer's disease amyloidosis models. *bioRxiv* **2020**.

31. Razansky, D.; Klohs, J.; Ni, R. Multi-scale optoacoustic molecular imaging of brain diseases. *Eur J Nucl Med Mol Imaging* **2021**, doi:10.1007/s00259-021-05207-4.

32. Jack, C.R., Jr.; Wengenack, T.M.; Reyes, D.A.; Garwood, M.; Curran, G.L.; Borowski, B.J.; Lin, J.; Preboske, G.M.; Holasek, S.S.; Adriany, G.; et al. In vivo magnetic resonance microimaging of individual amyloid plaques in Alzheimer's transgenic mice. *J Neurosci* **2005**, *25*, 10041-10048, doi:10.1523/jneurosci.2588-05.2005.

33. Maier, F.C.; Keller, M.D.; Bukala, D.; Bender, B.; Mannheim, J.G.; Brereton, I.M.; Galloway, G.J.; Pichler, B.J. Quantification of β-Amyloidosis and rCBF with Dedicated PET, 7 T MR Imaging, and High-Resolution Microscopic MR Imaging at 16.4 T in APP23 Mice. *J Nucl Med* **2015**, *56*, 1593-1599, doi:10.2967/jnumed.115.159350.

34. Bigot, C.; Vanhoutte, G.; Verhoye, M.; Van der Linden, A. Magnetization transfer contrast imaging reveals amyloid pathology in Alzheimer's disease transgenic mice. *NeuroImage* **2014**, *87*, 111-119, doi:https://doi.org/10.1016/j.neuroimage.2013.10.056.

35. Pérez-Torres, C.J.; Reynolds, J.O.; Pautler, R.G. Use of magnetization transfer contrast MRI to detect early molecular pathology in Alzheimer's disease. *Magn Reson Med* **2014**, *71*, 333-338, doi:10.1002/mrm.24665.

36. Jahng, G.H.; Choi, W.; Chung, J.J.; Kim, S.T.; Rhee, H.Y. Mapping Exchangeable Protons to Monitor Protein Alterations in the Brain of an Alzheimer's Disease Mouse Model by Using MRI. *Curr Alzheimer Res* **2018**, *15*, 1343-1353, doi:10.2174/1567205015666180911143518.

37. Kim, J.H.; Ha, T.L.; Im, G.H.; Yang, J.; Seo, S.W.; Chung, J.J.; Chae, S.Y.; Lee, I.S.; Lee, J.H. Magnetic resonance imaging for monitoring therapeutic response in a transgenic mouse model of Alzheimer's disease using voxel-based analysis of amyloid plaques. *Neuroreport* **2014**, *25*, 211-218, doi:10.1097/wnr.0000000000000067.

38. Li, L.; Wang, X.-Y.; Gao, F.-B.; Wang, L.; Xia, R.; Li, Z.-X.; Xing, W.; Tang, B.-S.; Zeng, Y.; Zhou, G.-F.; et al. Magnetic resonance T2 relaxation time at 7 Tesla associated with amyloid β pathology and age in a double-transgenic mouse model of Alzheimer's disease. *Neuroscience Letters* **2016**, *610*, 92-97, doi:https://doi.org/10.1016/j.neulet.2015.10.058.

39. El Tayara Nel, T.; Volk, A.; Dhenain, M.; Delatour, B. Transverse relaxation time reflects brain amyloidosis in young APP/PS1 transgenic mice. *Magn Reson Med* **2007**, *58*, 179-184, doi:10.1002/mrm.21266.

40. Fasae, K.D.; Abolaji, A.O.; Faloye, T.R.; Odunsi, A.Y.; Oyetayo, B.O.; Enya, J.I.; Rotimi, J.A.; Akinyemi, R.O.; Whitworth, A.J.; Aschner, M. Metallobiology and therapeutic chelation of biometals (copper, zinc and iron) in Alzheimer's disease: Limitations, and current and future perspectives. *Journal of Trace Elements in Medicine and Biology* **2021**, *67*, 126779, doi:https://doi.org/10.1016/j.jtemb.2021.126779.

41. Everett, J.; Lermyte, F.; Brooks, J.; Tjendana-Tjhin, V.; Plascencia-Villa, G.; Hands-Portman, I.; Donnelly, J.M.; Billimoria, K.; Perry, G.; Zhu, X.; et al. Biogenic metallic elements in the human brain? *Sci Adv* **2021**, *7*, doi:10.1126/sciadv.abf6707.

42. Gong, N.J.; Dibb, R.; Bulk, M.; van der Weerd, L.; Liu, C. Imaging beta amyloid aggregation and iron accumulation in Alzheimer's disease using quantitative susceptibility mapping MRI. *Neuroimage* **2019**, *191*, 176-185, doi:10.1016/j.neuroimage.2019.02.019.

43. Chamberlain, R.; Reyes, D.; Curran, G.L.; Marjanska, M.; Wengenack, T.M.; Poduslo, J.F.; Garwood, M.; Jack, C.R., Jr. Comparison of amyloid plaque contrast generated by T2-weighted, T2*-weighted, and susceptibility-weighted imaging methods in transgenic mouse models of Alzheimer's disease. *Magn Reson Med* **2009**, *61*, 1158-1164, doi:10.1002/mrm.21951.

44. Santin, M.D.; Vandenberghe, M.E.; Herard, A.S.; Pradier, L.; Cohen, C.; Debeir, T.; Delzescaux, T.; Rooney, T.; Dhenain, M. In Vivo Detection of Amyloid Plaques by Gadolinium-Stained MRI Can Be Used to Demonstrate the Efficacy of an Anti-amyloid Immunotherapy. *Front Aging Neurosci* **2016**, *8*, 55, doi:10.3389/fnagi.2016.00055.

45. Wadghiri, Y.Z.; Sigurdsson, E.M.; Sadowski, M.; Elliott, J.I.; Li, Y.; Scholtzova, H.; Tang, C.Y.; Aguinaldo, G.; Pappolla, M.; Duff, K.; et al. Detection of Alzheimer's amyloid in transgenic mice using magnetic resonance microimaging. *Magn Reson Med* **2003**, *50*, 293-302, doi:10.1002/mrm.10529.

46. Sigurdsson, E.M.; Wadghiri, Y.Z.; Mosconi, L.; Blind, J.A.; Knudsen, E.; Asuni, A.; Scholtzova, H.; Tsui, W.H.; Li, Y.; Sadowski, M.; et al. A non-toxic ligand for voxel-based MRI analysis of plaques in AD transgenic mice. *Neurobiology of aging* **2008**, *29*, 836-847, doi:10.1016/j.neurobiolaging.2006.12.018.

47. Wang, X.; Chan, H.N.; Desbois, N.; Gros, C.P.; Bolze, F.; Li, Y.; Li, H.W.; Wong, M.S. Multimodal Theranostic Cyanine-Conjugated Gadolinium(III) Complex for In Vivo Imaging of Amyloid-β in an Alzheimer's Disease Mouse Model. *ACS Appl Mater Interfaces* **2021**, *13*, 18525-18532, doi:10.1021/acsami.1c01585.

48. Badachhape, A.; Parekh, P.A.; Mu, Q.; Bhavane, R.; Srivastava, M.; Stupin, I.; Bhandari, P.; Devkota, L.; Tanifum, E.; Ghaghada, K.; et al. A novel MRI contrast agent for identifying hyperphosphorylative neurons as a marker of future tau pathology. *Alzheimer's & Dementia* **2020**, *16*, e041080, doi:https://doi.org/10.1002/alz.041080.

49. Wengenack, T.M.; Jack, C.R., Jr.; Garwood, M.; Poduslo, J.F. MR microimaging of amyloid plaques in Alzheimer's disease transgenic mice. *Eur J Nucl Med Mol Imaging* **2008**, *35 Suppl 1*, S82-88, doi:10.1007/s00259-007-0706-9.

50. Wadghiri, Y.Z.; Li, J.; Wang, J.; Hoang, D.M.; Sun, Y.; Xu, H.; Tsui, W.; Li, Y.; Boutajangout, A.; Wang, A.; et al. Detection of amyloid plaques targeted by bifunctional

USPIO in Alzheimer's disease transgenic mice using magnetic resonance microimaging. *PLoS One* **2013**, *8*, e57097, doi:10.1371/journal.pone.0057097.

51. Tafoya, M.A.; Madi, S.; Sillerud, L.O. Superparamagnetic nanoparticle-enhanced MRI of Alzheimer's disease plaques and activated microglia in 3X transgenic mouse brains: Contrast optimization. *J Magn Reson Imaging* **2017**, *46*, 574-588, doi:10.1002/jmri.25563.

52. Sillerud, L.O.; Solberg, N.O.; Chamberlain, R.; Orlando, R.A.; Heidrich, J.E.; Brown, D.C.; Brady, C.I.; Vander Jagt, T.A.; Garwood, M.; Vander Jagt, D.L. SPION-enhanced magnetic resonance imaging of Alzheimer's disease plaques in AβPP/PS-1 transgenic mouse brain. *J Alzheimers Dis* **2013**, *34*, 349-365, doi:10.3233/jad-121171.

53. Beckmann, N.; Gérard, C.; Abramowski, D.; Cannet, C.; Staufenbiel, M. Noninvasive magnetic resonance imaging detection of cerebral amyloid angiopathy-related microvascular alterations using superparamagnetic iron oxide particles in APP transgenic mouse models of Alzheimer's disease: application to passive Abeta immunotherapy. *J Neurosci* **2011**, *31*, 1023-1031, doi:10.1523/jneurosci.4936-10.2011.

54. Poduslo, J.F.; Hultman, K.L.; Curran, G.L.; Preboske, G.M.; Chamberlain, R.; Marjańska, M.; Garwood, M.; Jack, C.R., Jr.; Wengenack, T.M. Targeting vascular amyloid in arterioles of Alzheimer disease transgenic mice with amyloid β protein antibody-coated nanoparticles. *J Neuropathol Exp Neurol* **2011**, *70*, 653-661, doi:10.1097/NEN.0b013e318225038c.

55. Dudeffant, C.; Vandesquille, M.; Herbert, K.; Garin, C.M.; Alves, S.; Blanchard, V.; Comoy, E.E.; Petit, F.; Dhenain, M. Contrast-enhanced MR microscopy of amyloid plaques in five mouse models of amyloidosis and in human Alzheimer's disease brains. *Scientific reports* **2017**, *7*, 4955, doi:10.1038/s41598-017-05285-1.

56. Kim, E.; Di Censo, D.; Baraldo, M.; Simmons, C.; Rosa, I.; Randall, K.; Ballard, C.; Dickie, B.R.; Williams, S.C.R.; Killick, R.; et al. In vivo multi-parametric manganese-enhanced MRI for detecting amyloid plaques in rodent models of Alzheimer's disease. *Sci Rep* **2021**, *11*, 12419, doi:10.1038/s41598-021-91899-5.

57. Nasr, S.H.; Kouyoumdjian, H.; Mallett, C.; Ramadan, S.; Zhu, D.C.; Shapiro, E.M.; Huang, X. Detection of β-Amyloid by Sialic Acid Coated Bovine Serum Albumin Magnetic Nanoparticles in a Mouse Model of Alzheimer's Disease. *Small* **2018**, *14*, doi:10.1002/smll.201701828.

58. Higuchi, M.; Iwata, N.; Matsuba, Y.; Sato, K.; Sasamoto, K.; Saido, T.C. 19F and 1H MRI detection of amyloid beta plaques in vivo. *Nat Neurosci* **2005**, *8*, 527-533, doi:10.1038/nn1422.

59. Yousaf, M.; Ahmad, M.; Bhatti, I.A.; Nasir, A.; Hasan, M.; Jian, X.; Kalantar-Zadeh, K.; Mahmood, N. In Vivo and In Vitro Monitoring of Amyloid Aggregation via BSA@FGQDs Multimodal Probe. *ACS Sensors* **2019**, *4*, 200-210, doi:10.1021/acssensors.8b01216.

60. Amatsubo, T.; Morikawa, S.; Inubushi, T.; Urushitani, M.; Taguchi, H.; Shirai, N.; Hirao, K.; Kato, M.; Morino, K.; Kimura, H.; et al. Trifluoromethoxy-benzylated ligands improve amyloid detection in the brain using (19)F magnetic resonance imaging. *Neurosci Res* **2009**, *63*, 76-81, doi:10.1016/j.neures.2008.10.006.

61. Yanagisawa, D.; Ibrahim, N.F.; Taguchi, H.; Morikawa, S.; Tomiyama, T.; Tooyama, I. Fluorine-19 Magnetic Resonance Imaging for Detection of Amyloid β Oligomers Using a Keto Form of Curcumin Derivative in a Mouse Model of Alzheimer's Disease. *Molecules (Basel, Switzerland)* **2021**, *26*, 1362, doi:10.3390/molecules26051362.

62. Yanagisawa, D.; Amatsubo, T.; Morikawa, S.; Taguchi, H.; Urushitani, M.; Shirai, N.; Hirao, K.; Shiino, A.; Inubushi, T.; Tooyama, I. In vivo detection of amyloid β deposition using ^{19}F magnetic resonance imaging with a ^{19}F-containing curcumin derivative in a mouse model of Alzheimer's disease. *Neuroscience* **2011**, *184*, 120-127, doi:10.1016/j.neuroscience.2011.03.071.

63. Viola, K.L.; Sbarboro, J.; Sureka, R.; De, M.; Bicca, M.A.; Wang, J.; Vasavada, S.; Satpathy, S.; Wu, S.; Joshi, H.; et al. Towards non-invasive diagnostic imaging of early-stage Alzheimer's disease. *Nat Nanotechnol* **2015**, *10*, 91-98, doi:10.1038/nnano.2014.254.

64. Rozema, N.B.; Procissi, D.; Bertolino, N.; Viola, K.L.; Nandwana, V.; Abdul, N.; Pribus, S.; Dravid, V.; Klein, W.L.; Disterhoft, J.F.; et al. Aβ oligomer induced cognitive impairment and evaluation of ACU193-MNS-based MRI in rabbit. *Alzheimers Dement (N Y)* **2020**, *6*, e12087, doi:10.1002/trc2.12087.

65. Sehlin, D.; Fang, X.T.; Cato, L.; Antoni, G.; Lannfelt, L.; Syvänen, S. Antibody-based PET imaging of amyloid beta in mouse models of Alzheimer's disease. *Nat Commun* **2016**, *7*, 10759, doi:10.1038/ncomms10759.

66. Liu, X.G.; Zhang, L.; Lu, S.; Liu, D.Q.; Zhang, L.X.; Yu, X.L.; Liu, R.T. Multifunctional Superparamagnetic Iron Oxide Nanoparticles Conjugated with Aβ Oligomer-Specific scFv Antibody and Class A Scavenger Receptor Activator Show Early Diagnostic Potentials for Alzheimer's Disease. *Int J Nanomedicine* **2020**, *15*, 4919-4932, doi:10.2147/ijn.s240953.

67. Dong, C.M.; Guo, A.S.; To, A.; Chan, K.W.Y.; Chow, A.S.F.; Bian, L.; Leong, A.T.L.; Wu, E.X. Early Detection of Amyloid β Pathology in Alzheimer's Disease by Molecular MRI(). *Annu Int Conf IEEE Eng Med Biol Soc* **2020**, *2020*, 1100-1103, doi:10.1109/embc44109.2020.9176013.

68. Cheng, K.K.; Chan, P.S.; Fan, S.; Kwan, S.M.; Yeung, K.L.; Wáng, Y.X.; Chow, A.H.; Wu, E.X.; Baum, L. Curcumin-conjugated magnetic nanoparticles for detecting amyloid plaques in Alzheimer's disease mice using magnetic resonance imaging (MRI). *Biomaterials* **2015**, *44*, 155-172, doi:10.1016/j.biomaterials.2014.12.005.

69. Palop, J.J.; Chin, J.; Roberson, E.D.; Wang, J.; Thwin, M.T.; Bien-Ly, N.; Yoo, J.; Ho, K.O.; Yu, G.Q.; Kreitzer, A.; et al. Aberrant excitatory neuronal activity and compensatory remodeling of inhibitory hippocampal circuits in mouse models of Alzheimer's disease. *Neuron* **2007**, *55*, 697-711, doi:10.1016/j.neuron.2007.07.025.

70. Latif-Hernandez, A.; Sabanov, V.; Ahmed, T.; Craessaerts, K.; Saito, T.; Saido, T.; Balschun, D. The two faces of synaptic failure in App(NL-G-F) knock-in mice. *Alzheimers Res Ther* **2020**, *12*, 100, doi:10.1186/s13195-020-00667-6.

71. Jun, H.; Bramian, A.; Soma, S.; Saito, T.; Saido, T.C.; Igarashi, K.M. Disrupted Place Cell Remapping and Impaired Grid Cells in a Knockin Model of Alzheimer's Disease. *Neuron* **2020**, *107*, 1095-1112.e1096, doi:10.1016/j.neuron.2020.06.023.

72. Pervolaraki, E.; Hall, S.P.; Foresteire, D.; Saito, T.; Saido, T.C.; Whittington, M.A.; Lever, C.; Dachtler, J. Insoluble Aβ overexpression in an App knock-in mouse model alters microstructure and gamma oscillations in the prefrontal cortex, affecting anxiety-related behaviours. *Disease Models & Mechanisms* **2019**, *12*, doi:10.1242/dmm.040550.

73. Busche, M.A.; Eichhoff, G.; Adelsberger, H.; Abramowski, D.; Wiederhold, K.H.; Haass, C.; Staufenbiel, M.; Konnerth, A.; Garaschuk, O. Clusters of hyperactive neurons near amyloid

plaques in a mouse model of Alzheimer's disease. *Science* **2008**, *321*, 1686-1689, doi:10.1126/science.1162844.

74. Zott, B.; Simon, M.M.; Hong, W.; Unger, F.; Chen-Engerer, H.J.; Frosch, M.P.; Sakmann, B.; Walsh, D.M.; Konnerth, A. A vicious cycle of β amyloid-dependent neuronal hyperactivation. *Science* **2019**, *365*, 559-565, doi:10.1126/science.aay0198.

75. Tarantini, S.; Fulop, G.A.; Kiss, T.; Farkas, E.; Zölei-Szénási, D.; Galvan, V.; Toth, P.; Csiszar, A.; Ungvari, Z.; Yabluchanskiy, A. Demonstration of impaired neurovascular coupling responses in TG2576 mouse model of Alzheimer's disease using functional laser speckle contrast imaging. *Geroscience* **2017**, *39*, 465-473, doi:10.1007/s11357-017-9980-z.

76. Schroeder, M.P.; Weiss, C.; Procissi, D.; Wang, L.; Disterhoft, J.F. Activity-induced manganese-dependent MRI (AIM-MRI) and functional MRI in awake rabbits during somatosensory stimulation. *Neuroimage* **2016**, *126*, 72-80, doi:10.1016/j.neuroimage.2015.11.033.

77. Aoki, I.; Tanaka, C.; Takegami, T.; Ebisu, T.; Umeda, M.; Fukunaga, M.; Fukuda, K.; Silva, A.C.; Koretsky, A.P.; Naruse, S. Dynamic activity-induced manganese-dependent contrast magnetic resonance imaging (DAIM MRI). *Magn Reson Med* **2002**, *48*, 927-933, doi:10.1002/mrm.10320.

78. Androuin, A.; Abada, Y.-s.; Ly, M.; Santin, M.; Petiet, A.; Epelbaum, S.; Bertrand, A.; Delatour, B. Activity-induced MEMRI cannot detect functional brain anomalies in the APPxPS1-Ki mouse model of Alzheimer's disease. *Scientific Reports* **2019**, *9*, 1140, doi:10.1038/s41598-018-37980-y.

79. Yoshikawa, M.; Soeda, Y.; Michikawa, M.; Almeida, O.F.X.; Takashima, A. Tau Depletion in APP Transgenic Mice Attenuates Task-Related Hyperactivation of the Hippocampus and Differentially Influences Locomotor Activity and Spatial Memory. *Front Neurosci* **2018**, *12*, 124, doi:10.3389/fnins.2018.00124.

80. Nie, B.; Wu, D.; Liang, S.; Liu, H.; Sun, X.; Li, P.; Huang, Q.; Zhang, T.; Feng, T.; Ye, S.; et al. A stereotaxic MRI template set of mouse brain with fine sub-anatomical delineations: Application to MEMRI studies of 5XFAD mice. *Magn Reson Imaging* **2019**, *57*, 83-94, doi:10.1016/j.mri.2018.10.014.

81. Badea, A.; Delpratt, N.A.; Anderson, R.J.; Dibb, R.; Qi, Y.; Wei, H.; Liu, C.; Wetsel, W.C.; Avants, B.B.; Colton, C. Multivariate MR biomarkers better predict cognitive dysfunction in mouse models of Alzheimer's disease. *Magn Reson Imaging* **2019**, *60*, 52-67, doi:10.1016/j.mri.2019.03.022.

82. Saar, G.; Cheng, N.; Belluscio, L.; Koretsky, A.P. Laminar specific detection of APP induced neurodegeneration and recovery using MEMRI in an olfactory based Alzheimer's disease mouse model. *Neuroimage* **2015**, *118*, 183-192, doi:10.1016/j.neuroimage.2015.05.045.

83. Smith, K.D.B.; Kallhoff, V.; Zheng, H.; Pautler, R.G. In vivo axonal transport rates decrease in a mouse model of Alzheimer's disease. *NeuroImage* **2007**, *35*, 1401-1408, doi:10.1016/j.neuroimage.2007.01.046.

84. Wang, F.H.; Appelkvist, P.; Klason, T.; Gissberg, O.; Bogstedt, A.; Eliason, K.; Martinsson, S.; Briem, S.; Andersson, A.; Visser, S.A.; et al. Decreased axonal transport rates in the Tg2576 APP transgenic mouse: improvement with the gamma-secretase inhibitor MRK-560 as detected by manganese-enhanced MRI. *Eur J Neurosci* **2012**, *36*, 3165-3172, doi:10.1111/j.1460-9568.2012.08258.x.

85. Kim, J.; Choi, I.Y.; Michaelis, M.L.; Lee, P. Quantitative in vivo measurement of early axonal transport deficits in a triple transgenic mouse model of Alzheimer's disease using manganese-enhanced MRI. *Neuroimage* **2011**, *56*, 1286-1292, doi:10.1016/j.neuroimage.2011.02.039.

86. Medina, C.S.; Uselman, T.W.; Barto, D.R.; Cháves, F.; Jacobs, R.E.; Bearer, E.L. Decoupling the Effects of the Amyloid Precursor Protein From Amyloid-β Plaques on Axonal Transport Dynamics in the Living Brain. *Frontiers in Cellular Neuroscience* **2019**, *13*, 501.

87. Grandjean, J.; Canella, C.; Anckaerts, C.; Ayrancı, G.; Bougacha, S.; Bienert, T.; Buehlmann, D.; Coletta, L.; Gallino, D.; Gass, N.; et al. Common functional networks in the mouse brain revealed by multi-centre resting-state fMRI analysis. *Neuroimage* **2020**, *205*, 116278, doi:10.1016/j.neuroimage.2019.116278.

88. Logothetis, N.K.; Pauls, J.; Augath, M.; Trinath, T.; Oeltermann, A. Neurophysiological investigation of the basis of the fMRI signal. *Nature* **2001**, *412*, 150-157, doi:10.1038/35084005.

89. Polimeni, J.R.; Lewis, L.D. Imaging faster neural dynamics with fast fMRI: a need for updated models of the hemodynamic response. *Prog Neurobiol* **2021**, 102174, doi:10.1016/j.pneurobio.2021.102174.

90. Grandjean, J.; Schroeter, A.; He, P.; Tanadini, M.; Keist, R.; Krstic, D.; Konietzko, U.; Klohs, J.; Nitsch, R.M.; Rudin, M. Early alterations in functional connectivity and white matter structure in a transgenic mouse model of cerebral amyloidosis. *J Neurosci* **2014**, *34*, 13780-13789, doi:10.1523/jneurosci.4762-13.2014.

91. Shah, D.; Praet, J.; Latif Hernandez, A.; Höfling, C.; Anckaerts, C.; Bard, F.; Morawski, M.; Detrez, J.R.; Prinsen, E.; Villa, A.; et al. Early pathologic amyloid induces hypersynchrony of BOLD resting-state networks in transgenic mice and provides an early therapeutic window before amyloid plaque deposition. *Alzheimers Dement* **2016**, *12*, 964-976, doi:10.1016/j.jalz.2016.03.010.

92. Shah, D.; Latif-Hernandez, A.; Strooper, B.; Saito, T.; Saido, T.; Verhoye, M.; D'Hooge, R.; Van der Linden, A. Spatial reversal learning defect coincides with hypersynchronous telencephalic BOLD functional connectivity in APPNL-F/NL-F knock-in mice. *Scientific Reports* **2018**, *8*, doi:10.1038/s41598-018-24657-9.

93. Manno, F.A.M.; Isla, A.G.; Manno, S.H.C.; Ahmed, I.; Cheng, S.H.; Barrios, F.A.; Lau, C. Early Stage Alterations in White Matter and Decreased Functional Interhemispheric Hippocampal Connectivity in the 3xTg Mouse Model of Alzheimer's Disease. *Frontiers in Aging Neuroscience* **2019**, *11*, 39.

94. Grandjean, J.; Derungs, R.; Kulic, L.; Welt, T.; Henkelman, M.; Nitsch, R.M.; Rudin, M. Complex interplay between brain function and structure during cerebral amyloidosis in APP transgenic mouse strains revealed by multi-parametric MRI comparison. *Neuroimage* **2016**, *134*, 1-11, doi:10.1016/j.neuroimage.2016.03.042.

95. Sakurai, K.; Shintani, T.; Jomura, N.; Matsuda, T.; Sumiyoshi, A.; Hisatsune, T. Hyper BOLD Activation in Dorsal Raphe Nucleus of APP/PS1 Alzheimer's Disease Mouse during Reward-Oriented Drinking Test under Thirsty Conditions. *Scientific Reports* **2020**, *10*, 3915, doi:10.1038/s41598-020-60894-7.

96. Sanganahalli, B.G.; Herman, P.; Behar, K.L.; Blumenfeld, H.; Rothman, D.L.; Hyder, F. Functional MRI and neural responses in a rat model of Alzheimer's disease. *Neuroimage* **2013**, *79*, 404-411, doi:10.1016/j.neuroimage.2013.04.099.

97. Badea, A.; Kane, L.; Anderson, R.J.; Qi, Y.; Foster, M.; Cofer, G.P.; Medvitz, N.; Buckley, A.F.; Badea, A.K.; Wetsel, W.C.; et al. The fornix provides multiple biomarkers to characterize circuit disruption in a mouse model of Alzheimer's disease. *NeuroImage* **2016**, *142*, 498-511, doi:10.1016/j.neuroimage.2016.08.014.

98. Latif-Hernandez, A.; Shah, D.; Craessaerts, K.; Saido, T.; Saito, T.; De Strooper, B.; Van der Linden, A.; D'Hooge, R. Subtle behavioral changes and increased prefrontal-hippocampal network synchronicity in APP(NL-G-F) mice before prominent plaque deposition. *Behav Brain Res* **2019**, *364*, 431-441, doi:10.1016/j.bbr.2017.11.017.

99. Ben-Nejma, I.R.H.; Keliris, A.J.; Daans, J.; Ponsaerts, P.; Verhoye, M.; Van der Linden, A.; Keliris, G.A. Increased soluble amyloid-beta causes early aberrant brain network hypersynchronisation in a mature-onset mouse model of amyloidosis. *Acta Neuropathologica Communications* **2019**, *7*, 180, doi:10.1186/s40478-019-0810-7.

100. Shah, D.; Jonckers, E.; Praet, J.; Vanhoutte, G.; Delgado y Palacios, R.; Bigot, C.; D'Souza, D.V.; Verhoye, M.; Van der Linden, A. Resting State fMRI Reveals Diminished Functional Connectivity in a Mouse Model of Amyloidosis. *PLOS ONE* **2013**, *8*, e84241, doi:10.1371/journal.pone.0084241.

101. Gail Canter, R.; Huang, W.C.; Choi, H.; Wang, J.; Ashley Watson, L.; Yao, C.G.; Abdurrob, F.; Bousleiman, S.M.; Young, J.Z.; Bennett, D.A.; et al. 3D mapping reveals network-specific amyloid progression and subcortical susceptibility in mice. *Commun Biol* **2019**, *2*, 360, doi:10.1038/s42003-019-0599-8.

102. Tudela, R.; Muñoz-Moreno, E.; Sala-Llonch, R.; López-Gil, X.; Soria, G. Resting State Networks in the TgF344-AD Rat Model of Alzheimer's Disease Are Altered From Early Stages. *Front Aging Neurosci* **2019**, *11*, 213, doi:10.3389/fnagi.2019.00213.

103. Haller, S.; Zaharchuk, G.; Thomas, D.L.; Lovblad, K.O.; Barkhof, F.; Golay, X. Arterial Spin Labeling Perfusion of the Brain: Emerging Clinical Applications. *Radiology* **2016**, *281*, 337-356, doi:10.1148/radiol.2016150789.

104. Cruz Hernández, J.C.; Bracko, O.; Kersbergen, C.J.; Muse, V.; Haft-Javaherian, M.; Berg, M.; Park, L.; Vinarcsik, L.K.; Ivasyk, I.; Rivera, D.A.; et al. Neutrophil adhesion in brain capillaries reduces cortical blood flow and impairs memory function in Alzheimer's disease mouse models. *Nat Neurosci* **2019**, *22*, 413-420, doi:10.1038/s41593-018-0329-4.

105. Guo, Y.; Li, X.; Zhang, M.; Chen, N.; Wu, S.; Lei, J.; Wang, Z.; Wang, R.; Wang, J.; Liu, H. Age- and brain region-associated alterations of cerebral blood flow in early Alzheimer's disease assessed in AβPPSWE/PS1ΔE9 transgenic mice using arterial spin labeling. *Mol Med Rep* **2019**, *19*, 3045-3052, doi:10.3892/mmr.2019.9950.

106. Adlimoghaddam, A.; Snow, W.M.; Stortz, G.; Perez, C.; Djordjevic, J.; Goertzen, A.L.; Ko, J.H.; Albensi, B.C. Regional hypometabolism in the 3xTg mouse model of Alzheimer's disease. *Neurobiol Dis* **2019**, *127*, 264-277, doi:10.1016/j.nbd.2019.03.008.

107. Ni, R.; Kindler, D.R.; Waag, R.; Rouault, M.; Ravikumar, P.; Nitsch, R.; Rudin, M.; Camici, G.G.; Liberale, L.; Kulic, L.; et al. fMRI Reveals Mitigation of Cerebrovascular Dysfunction by Bradykinin Receptors 1 and 2 Inhibitor Noscapine in a Mouse Model of Cerebral Amyloidosis. *Frontiers in Aging Neuroscience* **2019**, *11*, 27.

108. Ni, R.; Rudin, M.; Klohs, J. Cortical hypoperfusion and reduced cerebral metabolic rate of oxygen in the arcAβ mouse model of Alzheimer's disease. *Photoacoustics* **2018**, *10*, 38-47, doi:https://doi.org/10.1016/j.pacs.2018.04.001.

109. Hébert, F.; Grand'maison, M.; Ho, M.K.; Lerch, J.P.; Hamel, E.; Bedell, B.J. Cortical atrophy and hypoperfusion in a transgenic mouse model of Alzheimer's disease. *Neurobiol Aging* **2013**, *34*, 1644-1652, doi:10.1016/j.neurobiolaging.2012.11.022.

110. Massaad, C.A.; Amin, S.K.; Hu, L.; Mei, Y.; Klann, E.; Pautler, R.G. Mitochondrial Superoxide Contributes to Blood Flow and Axonal Transport Deficits in the Tg2576 Mouse Model of Alzheimer's Disease. *PLOS ONE* **2010**, *5*, e10561, doi:10.1371/journal.pone.0010561.

111. Weidensteiner, C.; Metzger, F.; Bruns, A.; Bohrmann, B.; Kuennecke, B.; von Kienlin, M. Cortical hypoperfusion in the B6.PS2APP mouse model for Alzheimer's disease: comprehensive phenotyping of vascular and tissular parameters by MRI. *Magn Reson Med* **2009**, *62*, 35-45, doi:10.1002/mrm.21985.

112. Poisnel, G.; Hérard, A.S.; El Tannir El Tayara, N.; Bourrin, E.; Volk, A.; Kober, F.; Delatour, B.; Delzescaux, T.; Debeir, T.; Rooney, T.; et al. Increased regional cerebral glucose uptake in an APP/PS1 model of Alzheimer's disease. *Neurobiol Aging* **2012**, *33*, 1995-2005, doi:10.1016/j.neurobiolaging.2011.09.026.

113. Yezhuvath, U.S.; Uh, J.; Cheng, Y.; Martin-Cook, K.; Weiner, M.; Diaz-Arrastia, R.; van Osch, M.; Lu, H. Forebrain-dominant deficit in cerebrovascular reactivity in Alzheimer's disease. *Neurobiol Aging* **2012**, *33*, 75-82, doi:10.1016/j.neurobiolaging.2010.02.005.

114. Princz-Kranz, F.L.; Mueggler, T.; Knobloch, M.; Nitsch, R.M.; Rudin, M. Vascular response to acetazolamide decreases as a function of age in the arcA beta mouse model of cerebral amyloidosis. *Neurobiol Dis* **2010**, *40*, 284-292, doi:10.1016/j.nbd.2010.06.002.

115. Mueggler, T.; Baumann, D.; Rausch, M.; Staufenbiel, M.; Rudin, M. Age-dependent impairment of somatosensory response in the amyloid precursor protein 23 transgenic mouse model of Alzheimer's disease. *The Journal of neuroscience : the official journal of the Society for Neuroscience* **2003**, *23*, 8231-8236, doi:10.1523/JNEUROSCI.23-23-08231.2003.

116. Richiardi, J.; Monsch, A.U.; Haas, T.; Barkhof, F.; Van de Ville, D.; Radü, E.W.; Kressig, R.W.; Haller, S. Altered cerebrovascular reactivity velocity in mild cognitive impairment and Alzheimer's disease. *Neurobiol Aging* **2015**, *36*, 33-41, doi:10.1016/j.neurobiolaging.2014.07.020.

117. Cantin, S.; Villien, M.; Moreaud, O.; Tropres, I.; Keignart, S.; Chipon, E.; Le Bas, J.F.; Warnking, J.; Krainik, A. Impaired cerebral vasoreactivity to CO2 in Alzheimer's disease using BOLD fMRI. *Neuroimage* **2011**, *58*, 579-587, doi:10.1016/j.neuroimage.2011.06.070.

118. Beckmann, N.; Schuler, A.; Mueggler, T.; Meyer, E.P.; Wiederhold, K.-H.; Staufenbiel, M.; Krucker, T. Age-dependent cerebrovascular abnormalities and blood flow disturbances in APP23 mice modeling Alzheimer's disease. *The Journal of neuroscience : the official journal of the Society for Neuroscience* **2003**, *23*, 8453-8459, doi:10.1523/JNEUROSCI.23-24-08453.2003.

119. Wiesmann, M.; Zerbi, V.; Jansen, D.; Lütjohann, D.; Veltien, A.; Heerschap, A.; Kiliaan, A.J. Hypertension, cerebrovascular impairment, and cognitive decline in aged AβPP/PS1 mice. *Theranostics* **2017**, *7*, 1277-1289, doi:10.7150/thno.18509.

120. Govaerts, K.; Lechat, B.; Struys, T.; Kremer, A.; Borghgraef, P.; Van Leuven, F.; Himmelreich, U.; Dresselaers, T. Longitudinal assessment of cerebral perfusion and vascular response to hypoventilation in a bigenic mouse model of Alzheimer's disease with amyloid and tau pathology. *NMR in Biomedicine* **2019**, *32*, e4037, doi:https://doi.org/10.1002/nbm.4037.

121. Marjanska, M.; Curran, G.L.; Wengenack, T.M.; Henry, P.G.; Bliss, R.L.; Poduslo, J.F.; Jack, C.R., Jr.; Ugurbil, K.; Garwood, M. Monitoring disease progression in transgenic mouse models of Alzheimer's disease with proton magnetic resonance spectroscopy. *Proc Natl Acad Sci U S A* **2005**, *102*, 11906-11910, doi:10.1073/pnas.0505513102.

122. Westman, E.; Spenger, C.; Oberg, J.; Reyer, H.; Pahnke, J.; Wahlund, L.O. In vivo 1H-magnetic resonance spectroscopy can detect metabolic changes in APP/PS1 mice after donepezil treatment. *BMC Neurosci* **2009**, *10*, 33, doi:10.1186/1471-2202-10-33.

123. Shen, Z.; Lei, J.; Li, X.; Wang, Z.; Bao, X.; Wang, R. Multifaceted assessment of the APP/PS1 mouse model for Alzheimer's disease: Applying MRS, DTI, and ASL. *Brain Res* **2018**, *1698*, 114-120, doi:10.1016/j.brainres.2018.08.001.

124. Kuhla, A.; Rühlmann, C.; Lindner, T.; Polei, S.; Hadlich, S.; Krause, B.J.; Vollmar, B.; Teipel, S.J. APPswe/PS1dE9 mice with cortical amyloid pathology show a reduced NAA/Cr ratio without apparent brain atrophy: A MRS and MRI study. *NeuroImage: Clinical* **2017**, *15*, 581-586, doi:https://doi.org/10.1016/j.nicl.2017.06.009.

125. Liang, S.; Huang, J.; Liu, W.; Jin, H.; Li, L.; Zhang, X.; Nie, B.; Lin, R.; Tao, J.; Zhao, S.; et al. Magnetic resonance spectroscopy analysis of neurochemical changes in the atrophic hippocampus of APP/PS1 transgenic mice. *Behavioural Brain Research* **2017**, *335*, 26-31, doi:https://doi.org/10.1016/j.bbr.2017.08.005.

126. Marjańska, M.; Weigand, S.D.; Preboske, G.; Wengenack, T.M.; Chamberlain, R.; Curran, G.L.; Poduslo, J.F.; Garwood, M.; Kobayashi, D.; Lin, J.C.; et al. Treatment effects in a transgenic mouse model of Alzheimer's disease: a magnetic resonance spectroscopy study after passive immunization. *Neuroscience* **2014**, *259*, 94-100, doi:10.1016/j.neuroscience.2013.11.052.

127. Oberg, J.; Spenger, C.; Wang, F.H.; Andersson, A.; Westman, E.; Skoglund, P.; Sunnemark, D.; Norinder, U.; Klason, T.; Wahlund, L.O.; et al. Age related changes in brain metabolites observed by 1H MRS in APP/PS1 mice. *Neurobiol Aging* **2008**, *29*, 1423-1433, doi:10.1016/j.neurobiolaging.2007.03.002.

128. Kara, F.; Belloy, M.E.; Voncken, R.; Sarwari, Z.; Garima, Y.; Anckaerts, C.; Langbeen, A.; Leysen, V.; Shah, D.; Jacobs, J.; et al. Long-term ovarian hormone deprivation alters functional connectivity, brain neurochemical profile and white matter integrity in the Tg2576 amyloid mouse model of Alzheimer's disease. *Neurobiol Aging* **2021**, *102*, 139-150, doi:10.1016/j.neurobiolaging.2021.02.011.

129. Chiquita, S.; Ribeiro, M.; Castelhano, J.; Oliveira, F.; Sereno, J.; Batista, M.; Abrunhosa, A.; Rodrigues-Neves, A.C.; Carecho, R.; Baptista, F.; et al. A longitudinal multimodal in vivo molecular imaging study of the 3xTg-AD mouse model shows progressive early hippocampal and taurine loss. *Hum Mol Genet* **2019**, *28*, 2174-2188, doi:10.1093/hmg/ddz045.

130. Lee, M.; Lee, H.J.; Jeong, Y.J.; Oh, S.J.; Kang, K.J.; Han, S.J.; Nam, K.R.; Lee, Y.J.; Lee, K.C.; Ryu, Y.H.; et al. Age dependency of mGluR5 availability in 5xFAD mice measured by PET. *Neurobiol Aging* **2019**, *84*, 208-216, doi:10.1016/j.neurobiolaging.2019.08.006.

131. Micotti, E.; Paladini, A.; Balducci, C.; Tolomeo, D.; Frasca, A.; Marizzoni, M.; Filibian, M.; Caroli, A.; Valbusa, G.; Dix, S.; et al. Striatum and entorhinal cortex atrophy in AD mouse models: MRI comprehensive analysis. *Neurobiology of Aging* **2015**, *36*, 776-788, doi:https://doi.org/10.1016/j.neurobiolaging.2014.10.027.

132. Chaney, A.M.; Lopez-Picon, F.R.; Serrière, S.; Wang, R.; Bochicchio, D.; Webb, S.D.; Vandesquille, M.; Harte, M.K.; Georgiadou, C.; Lawrence, C.; et al. Prodromal neuroinflammatory, cholinergic and metabolite dysfunction detected by PET and MRS in the TgF344-AD transgenic rat model of AD: a collaborative multi-modal study. *Theranostics* **2021**, *11*, 6644-6667, doi:10.7150/thno.56059.

133. Tolomeo, D.; Micotti, E.; Serra, S.C.; Chappell, M.; Snellman, A.; Forloni, G. Chemical exchange saturation transfer MRI shows low cerebral 2-deoxy-D-glucose uptake in a model of Alzheimer's Disease. *Scientific Reports* **2018**, *8*, 9576, doi:10.1038/s41598-018-27839-7.

134. Huang, J.; van Zijl, P.C.M.; Han, X.; Dong, C.M.; Cheng, G.W.Y.; Tse, K.H.; Knutsson, L.; Chen, L.; Lai, J.H.C.; Wu, E.X.; et al. Altered d-glucose in brain parenchyma and cerebrospinal fluid of early Alzheimer's disease detected by dynamic glucose-enhanced MRI. *Sci Adv* **2020**, *6*, eaba3884, doi:10.1126/sciadv.aba3884.

135. Igarashi, H.; Ueki, S.; Kitaura, H.; Kera, T.; Ohno, K.; Ohkubo, M.; Terumitsu-Tsujita, M.; Kakita, A.; Kwee, I.L. Longitudinal GluCEST MRI Changes and Cerebral Blood Flow in 5xFAD Mice. *Contrast Media & Molecular Imaging* **2020**, *2020*, 8831936, doi:10.1155/2020/8831936.

136. Chen, L.; van Zijl, P.C.M.; Wei, Z.; Lu, H.; Duan, W.; Wong, P.C.; Li, T.; Xu, J. Early detection of Alzheimer's disease using creatine chemical exchange saturation transfer magnetic resonance imaging. *Neuroimage* **2021**, *236*, 118071, doi:10.1016/j.neuroimage.2021.118071.

137. Chen, L.; Wei, Z.; Chan, K.W.Y.; Cai, S.; Liu, G.; Lu, H.; Wong, P.C.; van Zijl, P.C.M.; Li, T.; Xu, J. Protein aggregation linked to Alzheimer's disease revealed by saturation transfer MRI. *Neuroimage* **2019**, *188*, 380-390, doi:10.1016/j.neuroimage.2018.12.018.

138. Iturria-Medina, Y.; Sotero, R.C.; Toussaint, P.J.; Mateos-Pérez, J.M.; Evans, A.C. Early role of vascular dysregulation on late-onset Alzheimer's disease based on multifactorial data-driven analysis. *Nat Commun* **2016**, *7*, 11934, doi:10.1038/ncomms11934.

139. Scheffer, S.; Hermkens, D.M.A.; van der Weerd, L.; de Vries, H.E.; Daemen, M.J.A.P. Vascular Hypothesis of Alzheimer Disease. *Arteriosclerosis, Thrombosis, and Vascular Biology* **2021**, *41*, 1265-1283, doi:10.1161/ATVBAHA.120.311911.

140. Turner, D.A.; Degan, S.; Hoffmann, U.; Galeffi, F.; Colton, C.A. CVN-AD Alzheimer's mice show premature reduction in neurovascular coupling in response to spreading depression and anoxia compared to aged controls. *Alzheimers Dement* **2021**, *17*, 1109-1120, doi:10.1002/alz.12289.

141. Zhang, X.; Yin, X.; Zhang, J.; Li, A.; Gong, H.; Luo, Q.; Zhang, H.; Gao, Z.; Jiang, H. High-resolution mapping of brain vasculature and its impairment in the hippocampus of Alzheimer's disease mice. *National Science Review* **2019**, *6*, 1223-1238, doi:10.1093/nsr/nwz124.

142. Merlini, M.; Meyer, E.P.; Ulmann-Schuler, A.; Nitsch, R.M. Vascular β-amyloid and early astrocyte alterations impair cerebrovascular function and cerebral metabolism in transgenic arcAβ mice. *Acta Neuropathol* **2011**, *122*, 293-311, doi:10.1007/s00401-011-0834-y.

143. Telling, N.D.; Everett, J.; Collingwood, J.F.; Dobson, J.; van der Laan, G.; Gallagher, J.J.; Wang, J.; Hitchcock, A.P. Iron Biochemistry is Correlated with Amyloid Plaque Morphology in an Established Mouse Model of Alzheimer's Disease. *Cell Chem Biol* **2017**, *24*, 1205-1215.e1203, doi:10.1016/j.chembiol.2017.07.014.

144. Beckmann, N.; Doelemeyer, A.; Zurbruegg, S.; Bigot, K.; Theil, D.; Frieauff, W.; Kolly, C.; Moulin, P.; Neddermann, D.; Kreutzer, R.; et al. Longitudinal noninvasive magnetic resonance imaging of brain microhemorrhages in BACE inhibitor–treated APP transgenic mice. *Neurobiology of Aging* **2016**, *45*, 50-60, doi:https://doi.org/10.1016/j.neurobiolaging.2016.05.009.

145. Maniskas, M.E.; Mack, A.F.; Morales-Scheihing, D.; Finger, C.; Zhu, L.; Paulter, R.; Urayama, A.; McCullough, L.D.; Manwani, B. Sex differences in a murine model of Cerebral Amyloid Angiopathy. *Brain, Behavior, & Immunity - Health* **2021**, *14*, 100260, doi:https://doi.org/10.1016/j.bbih.2021.100260.

146. Klohs, J.; Deistung, A.; Schweser, F.; Grandjean, J.; Dominietto, M.; Waschkies, C.; Nitsch, R.M.; Knuesel, I.; Reichenbach, J.R.; Rudin, M. Detection of cerebral microbleeds with quantitative susceptibility mapping in the ArcAbeta mouse model of cerebral amyloidosis. *J Cereb Blood Flow Metab* **2011**, *31*, 2282-2292, doi:10.1038/jcbfm.2011.118.

147. Klohs, J.; Politano, I.W.; Deistung, A.; Grandjean, J.; Drewek, A.; Dominietto, M.; Keist, R.; Schweser, F.; Reichenbach, J.R.; Nitsch, R.M.; et al. Longitudinal Assessment of Amyloid Pathology in Transgenic ArcAβ Mice Using Multi-Parametric Magnetic Resonance Imaging. *PLoS One* **2013**, *8*, e66097, doi:10.1371/journal.pone.0066097.

148. McIntosh, A.; Mela, V.; Harty, C.; Minogue, A.M.; Costello, D.A.; Kerskens, C.; Lynch, M.A. Iron accumulation in microglia triggers a cascade of events that leads to altered metabolism and compromised function in APP/PS1 mice. *Brain Pathol* **2019**, *29*, 606-621, doi:10.1111/bpa.12704.

149. Klohs, J.; Deistung, A.; Ielacqua, G.D.; Seuwen, A.; Kindler, D.; Schweser, F.; Vaas, M.; Kipar, A.; Reichenbach, J.R.; Rudin, M. Quantitative assessment of microvasculopathy in arcAβ mice with USPIO-enhanced gradient echo MRI. *J Cereb Blood Flow Metab* **2016**, *36*, 1614-1624, doi:10.1177/0271678x15621500.

150. Hilal, S.; Xu, X.; Ikram, M.K.; Vrooman, H.; Venketasubramanian, N.; Chen, C. Intracranial stenosis in cognitive impairment and dementia. *Journal of cerebral blood flow and metabolism : official journal of the International Society of Cerebral Blood Flow and Metabolism* **2017**, *37*, 2262-2269, doi:10.1177/0271678X16663752.

151. Roher, A.E.; Esh, C.; Rahman, A.; Kokjohn, T.A.; Beach, T.G. Atherosclerosis of cerebral arteries in Alzheimer disease. *Stroke* **2004**, *35*, 2623-2627, doi:10.1161/01.STR.0000143317.70478.b3.

152. Klohs, J.; Baltes, C.; Princz-Kranz, F.; Ratering, D.; Nitsch, R.M.; Knuesel, I.; Rudin, M. Contrast-enhanced magnetic resonance microangiography reveals remodeling of the cerebral microvasculature in transgenic ArcAβ mice. *J Neurosci* **2012**, *32*, 1705-1713, doi:10.1523/jneurosci.5626-11.2012.

153. Krucker, T.; Schuler, A.; Meyer, E.P.; Staufenbiel, M.; Beckmann, N. Magnetic resonance angiography and vascular corrosion casting as tools in biomedical research: application to transgenic mice modeling Alzheimer's disease. *Neurol Res* **2004**, *26*, 507-516, doi:10.1179/016164104225016281.

154. Ielacqua, G.D.; Schlegel, F.; Füchtemeier, M.; Xandry, J.; Rudin, M.; Klohs, J. Magnetic Resonance Q Mapping Reveals a Decrease in Microvessel Density in the arcAβ Mouse Model of Cerebral Amyloidosis. *Front Aging Neurosci* **2015**, *7*, 241, doi:10.3389/fnagi.2015.00241.

155. Chang, S.K.; Kim, J.; Lee, D.; Yoo, C.H.; Jin, S.; Rhee, H.Y.; Ryu, C.W.; Lee, J.K.; Cho, H.; Jahng, G.H. Mapping of microvascular architecture in the brain of an Alzheimer's disease mouse model using MRI. *NMR Biomed* **2021**, *34*, e4481, doi:10.1002/nbm.4481.

156. Leaston, J.; Ferris, C.F.; Kulkarni, P.; Chandramohan, D.; van de Ven, A.L.; Qiao, J.; Timms, L.; Sepulcre, J.; El Fakhri, G.; Ma, C.; et al. Neurovascular imaging with QUTE-CE MRI in APOE4 rats reveals early vascular abnormalities. *PLoS One* **2021**, *16*, e0256749, doi:10.1371/journal.pone.0256749.

157. Majumdar, S.; Klatt, D. Longitudinal study of sub-regional cerebral viscoelastic properties of 5XFAD Alzheimer's disease mice using multifrequency MR elastography. *Magn Reson Med* **2021**, *86*, 405-414, doi:10.1002/mrm.28709.

158. Munder, T.; Pfeffer, A.; Schreyer, S.; Guo, J.; Braun, J.; Sack, I.; Steiner, B.; Klein, C. MR elastography detection of early viscoelastic response of the murine hippocampus to amyloid β accumulation and neuronal cell loss due to Alzheimer's disease. *J Magn Reson Imaging* **2018**, *47*, 105-114, doi:10.1002/jmri.25741.

159. Murphy, M.C.; Curran, G.L.; Glaser, K.J.; Rossman, P.J.; Huston, J., 3rd; Poduslo, J.F.; Jack, C.R., Jr.; Felmlee, J.P.; Ehman, R.L. Magnetic resonance elastography of the brain in a mouse model of Alzheimer's disease: initial results. *Magn Reson Imaging* **2012**, *30*, 535-539, doi:10.1016/j.mri.2011.12.019.

160. Montagne, A.; Gauberti, M.; Macrez, R.; Jullienne, A.; Briens, A.; Raynaud, J.S.; Louin, G.; Buisson, A.; Haelewyn, B.; Docagne, F.; et al. Ultra-sensitive molecular MRI of cerebrovascular cell activation enables early detection of chronic central nervous system disorders. *Neuroimage* **2012**, *63*, 760-770, doi:10.1016/j.neuroimage.2012.07.018.

161. Badea, A.; Johnson, G.A.; Jankowsky, J.L. Remote sites of structural atrophy predict later amyloid formation in a mouse model of Alzheimer's disease. *NeuroImage* **2010**, *50*, 416-427, doi:10.1016/j.neuroimage.2009.12.070.

162. Kang, M.S.; Aliaga, A.A.; Shin, M.; Mathotaarachchi, S.; Benedet, A.L.; Pascoal, T.A.; Therriault, J.; Chamoun, M.; Savard, M.; Devenyi, G.A.; et al. Amyloid-beta modulates the association between neurofilament light chain and brain atrophy in Alzheimer's disease. *Molecular Psychiatry* **2020**, doi:10.1038/s41380-020-0818-1.

163. Van Broeck, B.; Vanhoutte, G.; Pirici, D.; Van Dam, D.; Wils, H.; Cuijt, I.; Vennekens, K.; Zabielski, M.; Michalik, A.; Theuns, J.; et al. Intraneuronal amyloid beta and reduced brain volume in a novel APP T714I mouse model for Alzheimer's disease. *Neurobiol Aging* **2008**, *29*, 241-252, doi:10.1016/j.neurobiolaging.2006.10.016.

164. Lau, J.C.; Lerch, J.P.; Sled, J.G.; Henkelman, R.M.; Evans, A.C.; Bedell, B.J. Longitudinal neuroanatomical changes determined by deformation-based morphometry in a mouse model of Alzheimer's disease. *Neuroimage* **2008**, *42*, 19-27, doi:10.1016/j.neuroimage.2008.04.252.

165. Kong, V.; Devenyi, G.A.; Gallino, D.; Ayranci, G.; Germann, J.; Rollins, C.; Chakravarty, M.M. Early-in-life neuroanatomical and behavioural trajectories in a triple transgenic model of Alzheimer's disease. *Brain Struct Funct* **2018**, *223*, 3365-3382, doi:10.1007/s00429-018-1691-4.

166. Breyhan, H.; Wirths, O.; Duan, K.; Marcello, A.; Rettig, J.; Bayer, T.A. APP/PS1KI bigenic mice develop early synaptic deficits and hippocampus atrophy. *Acta Neuropathol* **2009**, *117*, 677-685, doi:10.1007/s00401-009-0539-7.

167. Maheswaran, S.; Barjat, H.; Rueckert, D.; Bate, S.T.; Howlett, D.R.; Tilling, L.; Smart, S.C.; Pohlmann, A.; Richardson, J.C.; Hartkens, T.; et al. Longitudinal regional brain volume changes quantified in normal aging and Alzheimer's APP x PS1 mice using MRI. *Brain Res* **2009**, *1270*, 19-32, doi:10.1016/j.brainres.2009.02.045.

168. Delatour, B.; Guégan, M.; Volk, A.; Dhenain, M. In vivo MRI and histological evaluation of brain atrophy in APP/PS1 transgenic mice. *Neurobiology of Aging* **2006**, *27*, 835-847, doi:https://doi.org/10.1016/j.neurobiolaging.2005.04.011.

169. Badhwar, A.; Lerch, J.P.; Hamel, E.; Sled, J.G. Impaired structural correlates of memory in Alzheimer's disease mice. *Neuroimage Clin* **2013**, *3*, 290-300, doi:10.1016/j.nicl.2013.08.017.

170. Nasrabady, S.E.; Rizvi, B.; Goldman, J.E.; Brickman, A.M. White matter changes in Alzheimer's disease: a focus on myelin and oligodendrocytes. *Acta Neuropathologica Communications* **2018**, *6*, 22, doi:10.1186/s40478-018-0515-3.

171. Qin, Y.Y.; Li, M.W.; Zhang, S.; Zhang, Y.; Zhao, L.Y.; Lei, H.; Oishi, K.; Zhu, W.Z. In vivo quantitative whole-brain diffusion tensor imaging analysis of APP/PS1 transgenic mice using voxel-based and atlas-based methods. *Neuroradiology* **2013**, *55*, 1027-1038, doi:10.1007/s00234-013-1195-0.

172. Araque Caballero, M.Á.; Suárez-Calvet, M.; Duering, M.; Franzmeier, N.; Benzinger, T.; Fagan, A.M.; Bateman, R.J.; Jack, C.R.; Levin, J.; Dichgans, M.; et al. White matter diffusion alterations precede symptom onset in autosomal dominant Alzheimer's disease. *Brain : a journal of neurology* **2018**, *141*, 3065-3080, doi:10.1093/brain/awy229.

173. Chen, J.-F.; Liu, K.; Hu, B.; Li, R.-R.; Xin, W.; Chen, H.; Wang, F.; Chen, L.; Li, R.-X.; Ren, S.-Y.; et al. Enhancing myelin renewal reverses cognitive dysfunction in a murine model of Alzheimer's disease. *Neuron* **2021**, *109*, 2292-2307.e2295, doi:https://doi.org/10.1016/j.neuron.2021.05.012.

174. Depp, C.; Sun, T.; Sasmita, A.O.; Spieth, L.; Berghoff, S.; Steixner-Kumar, A.; Subramanian, S.; Möbius, W.; Göbbels, S.; Saher, G.; et al. Ageing-associated myelin dysfunction drives amyloid deposition in mouse models of Alzheimer's disease. **2021**, doi:10.1101/2021.07.31.454562.

175. Sun, S.W.; Song, S.K.; Harms, M.P.; Lin, S.J.; Holtzman, D.M.; Merchant, K.M.; Kotyk, J.J. Detection of age-dependent brain injury in a mouse model of brain amyloidosis associated with Alzheimer's disease using magnetic resonance diffusion tensor imaging. *Exp Neurol* **2005**, *191*, 77-85, doi:10.1016/j.expneurol.2004.09.006.

176. Song, S.K.; Kim, J.H.; Lin, S.J.; Brendza, R.P.; Holtzman, D.M. Diffusion tensor imaging detects age-dependent white matter changes in a transgenic mouse model with amyloid deposition. *Neurobiol Dis* **2004**, *15*, 640-647, doi:10.1016/j.nbd.2003.12.003.

177. Snow, W.M.; Dale, R.; O'Brien-Moran, Z.; Buist, R.; Peirson, D.; Martin, M.; Albensi, B.C. In Vivo Detection of Gray Matter Neuropathology in the 3xTg Mouse Model of Alzheimer's Disease with Diffusion Tensor Imaging. *J Alzheimers Dis* **2017**, *58*, 841-853, doi:10.3233/jad-170136.

178. Whittaker, H.T.; Zhu, S.; Di Curzio, D.L.; Buist, R.; Li, X.-M.; Noy, S.; Wiseman, F.K.; Thiessen, J.D.; Martin, M. T1, diffusion tensor, and quantitative magnetization transfer imaging of the hippocampus in an Alzheimer's disease mouse model. *Magnetic Resonance Imaging* **2018**, *50*, 26-37, doi:https://doi.org/10.1016/j.mri.2018.03.010.

179. Zerbi, V.; Kleinnijenhuis, M.; Fang, X.; Jansen, D.; Veltien, A.; Van Asten, J.; Timmer, N.; Dederen, P.J.; Kiliaan, A.J.; Heerschap, A. Gray and white matter degeneration revealed by diffusion in an Alzheimer mouse model. *Neurobiol Aging* **2013**, *34*, 1440-1450, doi:10.1016/j.neurobiolaging.2012.11.017.

180. Nie, X.; Falangola, M.F.; Ward, R.; McKinnon, E.T.; Helpern, J.A.; Nietert, P.J.; Jensen, J.H. Diffusion MRI detects longitudinal white matter changes in the 3xTg-AD mouse model of Alzheimer's disease. *Magn Reson Imaging* **2019**, *57*, 235-242, doi:10.1016/j.mri.2018.12.003.

181. Weishaupt, N.; Liu, Q.; Shin, S.; Singh, R.; Agca, Y.; Agca, C.; Hachinski, V.; Whitehead, S.N. APP21 transgenic rats develop age-dependent cognitive impairment and microglia accumulation within white matter tracts. *J Neuroinflammation* **2018**, *15*, 241, doi:10.1186/s12974-018-1273-7.

182. Hara, Y.; Motoi, Y.; Hikishima, K.; Mizuma, H.; Onoe, H.; Matsumoto, S.E.; Elahi, M.; Okano, H.; Aoki, S.; Hattori, N. Involvement of the Septo-Hippocampal Cholinergic Pathway in Association with Septal Acetylcholinesterase Upregulation in a Mouse Model of Tauopathy. *Curr Alzheimer Res* **2017**, *14*, 94-103, doi:10.2174/1567205013666160602235800.

183. Daianu, M.; Jacobs, R.E.; Weitz, T.M.; Town, T.C.; Thompson, P.M. Multi-Shell Hybrid Diffusion Imaging (HYDI) at 7 Tesla in TgF344-AD Transgenic Alzheimer Rats. *PLoS One* **2015**, *10*, e0145205, doi:10.1371/journal.pone.0145205.

184. Praet, J.; Manyakov, N.V.; Muchene, L.; Mai, Z.; Terzopoulos, V.; de Backer, S.; Torremans, A.; Guns, P.-J.; Van De Casteele, T.; Bottelbergs, A.; et al. Diffusion kurtosis imaging allows the early detection and longitudinal follow-up of amyloid-β-induced pathology. *Alzheimer's Research & Therapy* **2018**, *10*, 1, doi:10.1186/s13195-017-0329-8.

185. Neuner, S.M.; Heuer, S.E.; Huentelman, M.J.; O'Connell, K.M.S.; Kaczorowski, C.C. Harnessing Genetic Complexity to Enhance Translatability of Alzheimer's Disease Mouse Models: A Path toward Precision Medicine. *Neuron* **2019**, *101*, 399-411.e395, doi:10.1016/j.neuron.2018.11.040.

186. Müller, H.P.; Kassubek, J.; Vernikouskaya, I.; Ludolph, A.C.; Stiller, D.; Rasche, V. Diffusion tensor magnetic resonance imaging of the brain in APP transgenic mice: a cohort study. *PLoS One* **2013**, *8*, e67630, doi:10.1371/journal.pone.0067630.

187. Shu, X.; Qin, Y.Y.; Zhang, S.; Jiang, J.J.; Zhang, Y.; Zhao, L.Y.; Shan, D.; Zhu, W.Z. Voxel-based diffusion tensor imaging of an APP/PS1 mouse model of Alzheimer's disease. *Mol Neurobiol* **2013**, *48*, 78-83, doi:10.1007/s12035-013-8418-6.

188. Falangola, M.F.; Nie, X.; Ward, R.; Dhiman, S.; Voltin, J.; Nietert, P.J.; Jensen, J.H. Diffusion MRI detects basal forebrain cholinergic abnormalities in the 3xTg-AD mouse model of Alzheimer's disease. *Magn Reson Imaging* **2021**, *83*, 1-13, doi:10.1016/j.mri.2021.06.022.

189. Zhou, C.; Sun, X.; Hu, Y.; Song, J.; Dong, S.; Kong, D.; Wang, Y.; Hua, X.; Han, J.; Zhou, Y.; et al. Genomic deletion of TLR2 induces aggravated white matter damage and

deteriorated neurobehavioral functions in mouse models of Alzheimer's disease. *Aging (Albany NY)* **2019**, *11*, 7257-7273, doi:10.18632/aging.102260.

190. Kastyak-Ibrahim, M.Z.; Di Curzio, D.L.; Buist, R.; Herrera, S.L.; Albensi, B.C.; Del Bigio, M.R.; Martin, M. Neurofibrillary tangles and plaques are not accompanied by white matter pathology in aged triple transgenic-Alzheimer disease mice. *Magn Reson Imaging* **2013**, *31*, 1515-1521, doi:10.1016/j.mri.2013.06.013.

191. Mueggler, T.; Meyer-Luehmann, M.; Rausch, M.; Staufenbiel, M.; Jucker, M.; Rudin, M. Restricted diffusion in the brain of transgenic mice with cerebral amyloidosis. *European Journal of Neuroscience* **2004**, *20*, 811-817, doi:https://doi.org/10.1111/j.1460-9568.2004.03534.x.

192. Nishioka, C.; Liang, H.-F.; Barsamian, B.; Sun, S.-W. Amyloid-beta induced retrograde axonal degeneration in a mouse tauopathy model. *NeuroImage* **2019**, *189*, 180-191, doi:10.1016/j.neuroimage.2019.01.007.

193. Colon-Perez, L.M.; Ibanez, K.R.; Suarez, M.; Torroella, K.; Acuna, K.; Ofori, E.; Levites, Y.; Vaillancourt, D.E.; Golde, T.E.; Chakrabarty, P.; et al. Neurite orientation dispersion and density imaging reveals white matter and hippocampal microstructure changes produced by Interleukin-6 in the TgCRND8 mouse model of amyloidosis. *Neuroimage* **2019**, *202*, 116138, doi:10.1016/j.neuroimage.2019.116138.

194. Senatorov, V.V., Jr.; Friedman, A.R.; Milikovsky, D.Z.; Ofer, J.; Saar-Ashkenazy, R.; Charbash, A.; Jahan, N.; Chin, G.; Mihaly, E.; Lin, J.M.; et al. Blood-brain barrier dysfunction in aging induces hyperactivation of TGFβ signaling and chronic yet reversible neural dysfunction. *Sci Transl Med* **2019**, *11*, doi:10.1126/scitranslmed.aaw8283.

195. Sweeney, M.D.; Sagare, A.P.; Zlokovic, B.V. Blood-brain barrier breakdown in Alzheimer disease and other neurodegenerative disorders. *Nature reviews. Neurology* **2018**, *14*, 133-150, doi:10.1038/nrneurol.2017.188.

196. Nation, D.A.; Sweeney, M.D.; Montagne, A.; Sagare, A.P.; D'Orazio, L.M.; Pachicano, M.; Sepehrband, F.; Nelson, A.R.; Buennagel, D.P.; Harrington, M.G.; et al. Blood-brain barrier breakdown is an early biomarker of human cognitive dysfunction. *Nat Med* **2019**, *25*, 270-276, doi:10.1038/s41591-018-0297-y.

197. Montagne, A.; Nation, D.A.; Sagare, A.P.; Barisano, G.; Sweeney, M.D.; Chakhoyan, A.; Pachicano, M.; Joe, E.; Nelson, A.R.; D'Orazio, L.M.; et al. APOE4 leads to blood-brain barrier dysfunction predicting cognitive decline. *Nature* **2020**, *581*, 71-76, doi:10.1038/s41586-020-2247-3.

198. van de Haar, H.J.; Burgmans, S.; Jansen, J.F.; van Osch, M.J.; van Buchem, M.A.; Muller, M.; Hofman, P.A.; Verhey, F.R.; Backes, W.H. Blood-Brain Barrier Leakage in Patients with Early Alzheimer Disease. *Radiology* **2016**, *281*, 527-535, doi:10.1148/radiol.2016152244.

199. Ishii, M.; Iadecola, C. Risk factor for Alzheimer's disease breaks the blood-brain barrier. In *Nature*; 2020; Volume 581, pp. 31-32.

200. Bien-Ly, N.; Boswell, C.A.; Jeet, S.; Beach, T.G.; Hoyte, K.; Luk, W.; Shihadeh, V.; Ulufatu, S.; Foreman, O.; Lu, Y.; et al. Lack of Widespread BBB Disruption in Alzheimer's Disease Models: Focus on Therapeutic Antibodies. *Neuron* **2015**, *88*, 289-297, doi:10.1016/j.neuron.2015.09.036.

201. Montagne, A.; Barnes, S.R.; Sweeney, M.D.; Halliday, M.R.; Sagare, A.P.; Zhao, Z.; Toga, A.W.; Jacobs, R.E.; Liu, C.Y.; Amezcua, L.; et al. Blood-brain barrier breakdown in the aging human hippocampus. *Neuron* **2015**, *85*, 296-302, doi:10.1016/j.neuron.2014.12.032.

202. Montagne, A.; Nikolakopoulou, A.M.; Huuskonen, M.T.; Sagare, A.P.; Lawson, E.J.; Lazic, D.; Rege, S.V.; Grond, A.; Zuniga, E.; Barnes, S.R.; et al. APOE4 accelerates advanced-stage vascular and neurodegenerative disorder in old Alzheimer's mice via cyclophilin A independently of amyloid-β. *Nature Aging* **2021**, *1*, 506-520, doi:10.1038/s43587-021-00073-z.

203. Dickie, B.R.; Vandesquille, M.; Ulloa, J.; Boutin, H.; Parkes, L.M.; Parker, G.J.M. Water-exchange MRI detects subtle blood-brain barrier breakdown in Alzheimer's disease rats. *Neuroimage* **2019**, *184*, 349-358, doi:10.1016/j.neuroimage.2018.09.030.

204. Dickie, B.R.; Boutin, H.; Parker, G.J.M.; Parkes, L.M. Alzheimer's disease pathology is associated with earlier alterations to blood-brain barrier water permeability compared with healthy ageing in TgF344-AD rats. *NMR Biomed* **2021**, *34*, e4510, doi:10.1002/nbm.4510.

205. Iliff, J.J.; Wang, M.; Liao, Y.; Plogg, B.A.; Peng, W.; Gundersen, G.A.; Benveniste, H.; Vates, G.E.; Deane, R.; Goldman, S.A.; et al. A paravascular pathway facilitates CSF flow through the brain parenchyma and the clearance of interstitial solutes, including amyloid beta. *Sci Transl Med* **2012**, *4*, 147ra111, doi:10.1126/scitranslmed.3003748.

206. Nedergaard, M.; Goldman, S.A. Glymphatic failure as a final common pathway to dementia. *Science* **2020**, *370*, 50-56, doi:10.1126/science.abb8739.

207. Xie, L.; Kang, H.; Xu, Q.; Chen, M.J.; Liao, Y.; Thiyagarajan, M.; O'Donnell, J.; Christensen, D.J.; Nicholson, C.; Iliff, J.J.; et al. Sleep drives metabolite clearance from the adult brain. *Science* **2013**, *342*, 373-377, doi:10.1126/science.1241224.

208. Hawkes, C.A.; Härtig, W.; Kacza, J.; Schliebs, R.; Weller, R.O.; Nicoll, J.A.; Carare, R.O. Perivascular drainage of solutes is impaired in the ageing mouse brain and in the presence of cerebral amyloid angiopathy. *Acta Neuropathol* **2011**, *121*, 431-443, doi:10.1007/s00401-011-0801-7.

209. Da Mesquita, S.; Louveau, A.; Vaccari, A.; Smirnov, I.; Cornelison, R.C.; Kingsmore, K.M.; Contarino, C.; Onengut-Gumuscu, S.; Farber, E.; Raper, D.; et al. Functional aspects of meningeal lymphatics in ageing and Alzheimer's disease. *Nature* **2018**, *560*, 185-191, doi:10.1038/s41586-018-0368-8.

210. Da Mesquita, S.; Papadopoulos, Z.; Dykstra, T.; Brase, L.; Farias, F.G.; Wall, M.; Jiang, H.; Kodira, C.D.; de Lima, K.A.; Herz, J.; et al. Meningeal lymphatics affect microglia responses and anti-Aβ immunotherapy. *Nature* **2021**, *593*, 255-260, doi:10.1038/s41586-021-03489-0.

211. Ringstad, G.; Vatnehol, S.A.S.; Eide, P.K. Glymphatic MRI in idiopathic normal pressure hydrocephalus. *Brain* **2017**, *140*, 2691-2705, doi:10.1093/brain/awx191.

212. Watts, R.; Steinklein, J.M.; Waldman, L.; Zhou, X.; Filippi, C.G. Measuring Glymphatic Flow in Man Using Quantitative Contrast-Enhanced MRI. *AJNR Am J Neuroradiol* **2019**, *40*, 648-651, doi:10.3174/ajnr.A5931.

213. Harrison, I.F.; Ismail, O.; Machhada, A.; Colgan, N.; Ohene, Y.; Nahavandi, P.; Ahmed, Z.; Fisher, A.; Meftah, S.; Murray, T.K.; et al. Impaired glymphatic function and clearance of tau in an Alzheimer's disease model. *Brain* **2020**, *143*, 2576-2593, doi:10.1093/brain/awaa179.

214. Lee, H.; Mortensen, K.; Sanggaard, S.; Koch, P.; Brunner, H.; Quistorff, B.; Nedergaard, M.; Benveniste, H. Quantitative Gd-DOTA uptake from cerebrospinal fluid into rat brain using 3D VFA-SPGR at 9.4T. *Magn Reson Med* **2018**, *79*, 1568-1578, doi:10.1002/mrm.26779.

215. Iliff, J.J.; Lee, H.; Yu, M.; Feng, T.; Logan, J.; Nedergaard, M.; Benveniste, H. Brain-wide pathway for waste clearance captured by contrast-enhanced MRI. *J Clin Invest* **2013**, *123*, 1299-1309, doi:10.1172/jci67677.

216. Lee, H.; Xie, L.; Yu, M.; Kang, H.; Feng, T.; Deane, R.; Logan, J.; Nedergaard, M.; Benveniste, H. The Effect of Body Posture on Brain Glymphatic Transport. *J Neurosci* **2015**, *35*, 11034-11044, doi:10.1523/jneurosci.1625-15.2015.

217. Harrison, I.F.; Siow, B.; Akilo, A.B.; Evans, P.G.; Ismail, O.; Ohene, Y.; Nahavandi, P.; Thomas, D.L.; Lythgoe, M.F.; Wells, J.A. Non-invasive imaging of CSF-mediated brain clearance pathways via assessment of perivascular fluid movement with diffusion tensor MRI. *Elife* **2018**, *7*, doi:10.7554/eLife.34028.

218. Taoka, T.; Masutani, Y.; Kawai, H.; Nakane, T.; Matsuoka, K.; Yasuno, F.; Kishimoto, T.; Naganawa, S. Evaluation of glymphatic system activity with the diffusion MR technique: diffusion tensor image analysis along the perivascular space (DTI-ALPS) in Alzheimer's disease cases. *Japanese Journal of Radiology* **2017**, *35*, 172-178, doi:10.1007/s11604-017-0617-z.

219. Li, A.M.; Xu, J. Interstitial and cerebrospinal fluid exchanging process revealed by phase alternate labeling with null recovery MRI. *bioRxiv* **2021**, 2021.2007.2026.453795, doi:10.1101/2021.07.26.453795.

220. Ahmed, T.; He, C.; Abbasi, A.; Li, L.; Foltz, W.; Cai, P.; Knock, E.; Fraser, P.; Rauth, A.; Henderson, J.; et al. Multifunctional bioreactive-nanoconstructs for sensitive and accurate MRI of cerebrospinal fluid pathology and intervention of Alzheimer's disease. *Nano Today* **2020**, *35*, 100965, doi:10.1016/j.nantod.2020.100965.

221. Spencer, N.G.; Bridges, L.R.; Elderfield, K.; Amir, K.; Austen, B.; Howe, F.A. Quantitative evaluation of MRI and histological characteristics of the 5xFAD Alzheimer mouse brain. *NeuroImage* **2013**, *76*, 108-115, doi:https://doi.org/10.1016/j.neuroimage.2013.02.071.

222. Falangola, M.F.; Dyakin, V.V.; Lee, S.P.; Bogart, A.; Babb, J.S.; Duff, K.; Nixon, R.; Helpern, J.A. Quantitative MRI reveals aging-associated T2 changes in mouse models of Alzheimer's disease. *NMR Biomed* **2007**, *20*, 343-351, doi:10.1002/nbm.1163.

223. Helpern, J.A.; Lee, S.P.; Falangola, M.F.; Dyakin, V.V.; Bogart, A.; Ardekani, B.; Duff, K.; Branch, C.; Wisniewski, T.; de Leon, M.J.; et al. MRI assessment of neuropathology in a transgenic mouse model of Alzheimer's disease. *Magn Reson Med* **2004**, *51*, 794-798, doi:10.1002/mrm.20038.

224. Braakman, N.; Matysik, J.; van Duinen, S.G.; Verbeek, F.; Schliebs, R.; de Groot, H.J.; Alia, A. Longitudinal assessment of Alzheimer's beta-amyloid plaque development in transgenic mice monitored by in vivo magnetic resonance microimaging. *J Magn Reson Imaging* **2006**, *24*, 530-536, doi:10.1002/jmri.20675.

225. Wengenack, T.M.; Reyes, D.A.; Curran, G.L.; Borowski, B.J.; Lin, J.; Preboske, G.M.; Holasek, S.S.; Gilles, E.J.; Chamberlain, R.; Marjanska, M.; et al. Regional differences in MRI detection of amyloid plaques in AD transgenic mouse brain. *Neuroimage* **2011**, *54*, 113-122, doi:10.1016/j.neuroimage.2010.08.033.

226. Vanhoutte, G.; Dewachter, I.; Borghgraef, P.; Van Leuven, F.; Van der Linden, A. Noninvasive in vivo MRI detection of neuritic plaques associated with iron in APP[V717I] transgenic mice, a model for Alzheimer's disease. *Magn Reson Med* **2005**, *53*, 607-613, doi:10.1002/mrm.20385.

227. Raymond, S.B.; Treat, L.H.; Dewey, J.D.; McDannold, N.J.; Hynynen, K.; Bacskai, B.J. Ultrasound enhanced delivery of molecular imaging and therapeutic agents in Alzheimer's disease mouse models. *PLoS One* **2008**, *3*, e2175, doi:10.1371/journal.pone.0002175.

228. Dhenain, M.; El Tannir El Tayara, N.; Wu, T.D.; Guégan, M.; Volk, A.; Quintana, C.; Delatour, B. Characterization of in vivo MRI detectable thalamic amyloid plaques from APP/PS1 mice. *Neurobiol Aging* **2009**, *30*, 41-53, doi:10.1016/j.neurobiolaging.2007.05.018.

229. Faber, C.; Zahneisen, B.; Tippmann, F.; Schroeder, A.; Fahrenholz, F. Gradient-echo and CRAZED imaging for minute detection of Alzheimer plaques in an APPV717I x ADAM10-dn mouse model. *Magn Reson Med* **2007**, *57*, 696-703, doi:10.1002/mrm.21201.

230. Luo, F.; Rustay, N.R.; Ebert, U.; Hradil, V.P.; Cole, T.B.; Llano, D.A.; Mudd, S.R.; Zhang, Y.; Fox, G.B.; Day, M. Characterization of 7- and 19-month-old Tg2576 mice using multimodal in vivo imaging: limitations as a translatable model of Alzheimer's disease. *Neurobiol Aging* **2012**, *33*, 933-944, doi:10.1016/j.neurobiolaging.2010.08.005.

231. Anckaerts, C.; Blockx, I.; Summer, P.; Michael, J.; Hamaide, J.; Kreutzer, C.; Boutin, H.; Couillard-Després, S.; Verhoye, M.; Van der Linden, A. Early functional connectivity deficits and progressive microstructural alterations in the TgF344-AD rat model of Alzheimer's Disease: A longitudinal MRI study. *Neurobiology of Disease* **2019**, *124*, 93-107, doi:https://doi.org/10.1016/j.nbd.2018.11.010.

232. Parent, M.J.; Zimmer, E.R.; Shin, M.; Kang, M.S.; Fonov, V.S.; Mathieu, A.; Aliaga, A.; Kostikov, A.; Do Carmo, S.; Dea, D.; et al. Multimodal Imaging in Rat Model Recapitulates Alzheimer's Disease Biomarkers Abnormalities. *J Neurosci* **2017**, *37*, 12263-12271, doi:10.1523/jneurosci.1346-17.2017.

233. Lourenço, C.F.; Ledo, A.; Barbosa, R.M.; Laranjinha, J. Neurovascular uncoupling in the triple transgenic model of Alzheimer's disease: Impaired cerebral blood flow response to neuronal-derived nitric oxide signaling. *Experimental Neurology* **2017**, *291*, 36-43, doi:https://doi.org/10.1016/j.expneurol.2017.01.013.

234. Li, H.; Guo, Q.; Inoue, T.; Polito, V.A.; Tabuchi, K.; Hammer, R.E.; Pautler, R.G.; Taffet, G.E.; Zheng, H. Vascular and parenchymal amyloid pathology in an Alzheimer disease knock-in mouse model: interplay with cerebral blood flow. *Molecular neurodegeneration* **2014**, *9*, 28-28, doi:10.1186/1750-1326-9-28.

235. Maier, F.C.; Wehrl, H.F.; Schmid, A.M.; Mannheim, J.G.; Wiehr, S.; Lerdkrai, C.; Calaminus, C.; Stahlschmidt, A.; Ye, L.; Burnet, M.; et al. Longitudinal PET-MRI reveals β-amyloid deposition and rCBF dynamics and connects vascular amyloidosis to quantitative loss of perfusion. *Nature Medicine* **2014**, *20*, 1485-1492, doi:10.1038/nm.3734.

236. Poisnel, G.; Dhilly, M.; Moustié, O.; Delamare, J.; Abbas, A.; Guilloteau, D.; Barré, L. PET imaging with [18F]AV-45 in an APP/PS1-21 murine model of amyloid plaque deposition. *Neurobiol Aging* **2012**, *33*, 2561-2571, doi:10.1016/j.neurobiolaging.2011.12.024.

237. Patrick, D.-M.; Joël, L.; Pier-Luc, T.; Bernard, I.L.; Philippe, P.; Frédéric, L. Whole brain vascular imaging in a mouse model of Alzheimer's disease with two-photon microscopy. *Journal of Biomedical Optics* **2018**, *23*, 1-10, doi:10.1117/1.JBO.23.7.076501.

238. Hooijmans, C.R.; Graven, C.; Dederen, P.J.; Tanila, H.; van Groen, T.; Kiliaan, A.J. Amyloid beta deposition is related to decreased glucose transporter-1 levels and hippocampal atrophy in brains of aged APP/PS1 mice. *Brain Res* **2007**, *1181*, 93-103, doi:10.1016/j.brainres.2007.08.063.

239. Faure, A.; Verret, L.; Bozon, B.; El Tannir El Tayara, N.; Ly, M.; Kober, F.; Dhenain, M.; Rampon, C.; Delatour, B. Impaired neurogenesis, neuronal loss, and brain functional deficits in the APPxPS1-Ki mouse model of Alzheimer's disease. *Neurobiol Aging* **2011**, *32*, 407-418, doi:10.1016/j.neurobiolaging.2009.03.009.

240. Munting, L.P.; Derieppe, M.; Suidgeest, E.; Hirschler, L.; van Osch, M.J.; Denis de Senneville, B.; van der Weerd, L. Cerebral blood flow and cerebrovascular reactivity are preserved in a mouse model of cerebral microvascular amyloidosis. *Elife* **2021**, *10*, doi:10.7554/eLife.61279.

241. Li, M.; Kitamura, A.; Beverley, J.; Koudelka, J.; Duncombe, J.; Platt, B.; Wiegand, U.K.; Carare, R.O.; Kalaria, R.N.; Iliff, J.J.; et al. Pulsation changes link to impaired glymphatic function in a mouse model of vascular cognitive impairment. *bioRxiv* **2021**, 2021.2006.2008.447375, doi:10.1101/2021.06.08.447375.

242. Macdonald, I.R.; DeBay, D.R.; Reid, G.A.; O'Leary, T.P.; Jollymore, C.T.; Mawko, G.; Burrell, S.; Martin, E.; Bowen, C.V.; Brown, R.E.; et al. Early detection of cerebral glucose uptake changes in the 5XFAD mouse. *Curr Alzheimer Res* **2014**, *11*, 450-460, doi:10.2174/1567205011666140505111354.

243. Nizari, S.; Wells, J.A.; Carare, R.O.; Romero, I.A.; Hawkes, C.A. Loss of cholinergic innervation differentially affects eNOS-mediated blood flow, drainage of Aβ and cerebral amyloid angiopathy in the cortex and hippocampus of adult mice. *Acta Neuropathologica Communications* **2021**, *9*, 12, doi:10.1186/s40478-020-01108-z.

244. Wei, Z.; Xu, J.; Chen, L.; Hirschler, L.; Barbier, E.L.; Li, T.; Wong, P.C.; Lu, H. Brain metabolism in tau and amyloid mouse models of Alzheimer's disease: An MRI study. *NMR Biomed* **2021**, e4568, doi:10.1002/nbm.4568.

245. Do, T.M.; Alata, W.; Dodacki, A.; Traversy, M.T.; Chacun, H.; Pradier, L.; Scherrmann, J.M.; Farinotti, R.; Calon, F.; Bourasset, F. Altered cerebral vascular volumes and solute transport at the blood-brain barriers of two transgenic mouse models of Alzheimer's disease. *Neuropharmacology* **2014**, *81*, 311-317, doi:10.1016/j.neuropharm.2014.02.010.

246. Thal, D.R.; Capetillo-Zarate, E.; Larionov, S.; Staufenbiel, M.; Zurbruegg, S.; Beckmann, N. Capillary cerebral amyloid angiopathy is associated with vessel occlusion and cerebral blood flow disturbances. *Neurobiol Aging* **2009**, *30*, 1936-1948, doi:10.1016/j.neurobiolaging.2008.01.017.

247. Wu, C.C.; Chawla, F.; Games, D.; Rydel, R.E.; Freedman, S.; Schenk, D.; Young, W.G.; Morrison, J.H.; Bloom, F.E. Selective vulnerability of dentate granule cells prior to amyloid deposition in PDAPP mice: digital morphometric analyses. *Proc Natl Acad Sci U S A* **2004**, *101*, 7141-7146, doi:10.1073/pnas.0402147101.

248. Moreno, H.; Wu, W.E.; Lee, T.; Brickman, A.; Mayeux, R.; Brown, T.R.; Small, S.A. Imaging the Abeta-related neurotoxicity of Alzheimer disease. *Arch Neurol* **2007**, *64*, 1467-1477, doi:10.1001/archneur.64.10.1467.

249. Baligand, C.; Barret, O.; Tourais, A.; Pérot, J.B.; Thenadey, D.; Petit, F.; Liot, G.; Gaillard, M.C.; Flament, J.; Dhenain, M.; et al. Zero Echo Time (17)O-MRI Reveals Decreased

Cerebral Metabolic Rate of Oxygen Consumption in a Murine Model of Amyloidosis. *Metabolites* **2021**, *11*, doi:10.3390/metabo11050263.

250. Redwine, J.M.; Kosofsky, B.; Jacobs, R.E.; Games, D.; Reilly, J.F.; Morrison, J.H.; Young, W.G.; Bloom, F.E. Dentate gyrus volume is reduced before onset of plaque formation in PDAPP mice: a magnetic resonance microscopy and stereologic analysis. *Proc Natl Acad Sci U S A* **2003**, *100*, 1381-1386, doi:10.1073/pnas.242746599.

251. Weiss, C.; Venkatasubramanian, P.; Aguado, A.; Power, J.; Tom, B.; Li, L.; Chen, K.; Disterhoft, J.; Wyrwicz, A. Impaired Eyeblink Conditioning and Decreased Hippocampal Volume in PDAPP V717F Mice. *Neurobiology of disease* **2003**, *11*, 425-433, doi:10.1006/nbdi.2002.0555.

252. Van Broeck, B.; Vanhoutte, G.; Pirici, D.; Van Dam, D.; Wils, H.; Cuijt, I.; Vennekens, K.l.; Zabielski, M.; Michalik, A.; Theuns, J.; et al. Intraneuronal amyloid β and reduced brain volume in a novel APP T714I mouse model for Alzheimer's disease. *Neurobiology of aging* **2008**, *29*, 241-252, doi:10.1016/j.neurobiolaging.2006.10.016.

253. Rollins, C.P.E.; Gallino, D.; Kong, V.; Ayranci, G.; Devenyi, G.A.; Germann, J.; Chakravarty, M.M. Contributions of a high-fat diet to Alzheimer's disease-related decline: A longitudinal behavioural and structural neuroimaging study in mouse models. *NeuroImage. Clinical* **2019**, *21*, 101606, doi:10.1016/j.nicl.2018.11.016.

254. Badea, A.; Gewalt, S.; Avants, B.B.; Cook, J.J.; Johnson, G.A. Quantitative mouse brain phenotyping based on single and multispectral MR protocols. *Neuroimage* **2012**, *63*, 1633-1645, doi:10.1016/j.neuroimage.2012.07.021.

255. Song, S.K.; Yoshino, J.; Le, T.Q.; Lin, S.J.; Sun, S.W.; Cross, A.H.; Armstrong, R.C. Demyelination increases radial diffusivity in corpus callosum of mouse brain. *Neuroimage* **2005**, *26*, 132-140, doi:10.1016/j.neuroimage.2005.01.028.

256. Shepherd, T.M.; Ozarslan, E.; King, M.A.; Mareci, T.H.; Blackband, S.J. Structural insights from high-resolution diffusion tensor imaging and tractography of the isolated rat hippocampus. *Neuroimage* **2006**, *32*, 1499-1509, doi:10.1016/j.neuroimage.2006.04.210.

257. Bittner, T.; Fuhrmann, M.; Burgold, S.; Ochs, S.M.; Hoffmann, N.; Mitteregger, G.; Kretzschmar, H.; LaFerla, F.M.; Herms, J. Multiple Events Lead to Dendritic Spine Loss in Triple Transgenic Alzheimer's Disease Mice. *PLOS ONE* **2010**, *5*, e15477, doi:10.1371/journal.pone.0015477.

258. Falangola, M.F.; Nie, X.; Ward, R.; McKinnon, E.T.; Dhiman, S.; Nietert, P.J.; Helpern, J.A.; Jensen, J.H. Diffusion MRI detects early brain microstructure abnormalities in 2-month-old 3×Tg-AD mice. *NMR in Biomedicine* **2020**, *33*, e4346, doi:https://doi.org/10.1002/nbm.4346.

259. El Tayara Nel, T.; Delatour, B.; Volk, A.; Dhenain, M. Detection of vascular alterations by in vivo magnetic resonance angiography and histology in APP/PS1 mouse model of Alzheimer's disease. *Magma* **2010**, *23*, 53-64, doi:10.1007/s10334-009-0194-y.

260. Kara, F.; van Dongen, E.S.; Schliebs, R.; van Buchem, M.A.; de Groot, H.J.M.; Alia, A. Monitoring blood flow alterations in the Tg2576 mouse model of Alzheimer's disease by in vivo magnetic resonance angiography at 17.6T. *NeuroImage* **2012**, *60*, 958-966, doi:https://doi.org/10.1016/j.neuroimage.2011.12.055.

Preprints (www.preprints.org) | NOT PEER-REVIEWED | Posted: 15 October 2021 doi:10.20944/preprints202110.0231.v1

Table 1. MRI for detecting cerebral Aβ deposits in animal models of amyloidosis

MRI endogenous contrast	Animal	References
T_2, relaxation time	5×FAD, APP, APP/PS1, APPswe PS mice	[38,39] [221-224]
3D GRE, T_2* 16.4T	APP23 mice	[33]
T_2*w GE, T_2w SE	APP/PS1, APP_{V717I} mice	[32,49,225,226]
CESL	APP/PS1 mice	[36]
T_1w, CE-MR	APP/PS1, PDAPP mice	[227]
3D GE T_2*w	APP/PS1, PS1 mice	[228]
MTC	APP/PS1 mice	[34,35]
CRAZED, GE	APP_{V717I}×ADAM10-dn mice	[229]
QSM, SWI	Tg-SwDI, APP/PS1 mice	[42,43]
MRI, Contrast agents	**Animal**	**References**
^{19}F, BSA@FGQDs	AD mice	[59]
^{19}F, TFMB	APP mice	[60]
^{19}F, ^{1}H, FSB	APPswe mice	[58]
^{19}F, Shiga-Y51	APP/PS1 mice	[61]
^{19}F, FMeC1 (Shiga-Y5)	APPswe mice	[62]
T_2*w, Sialic acid coated BSA MNP	APP/PS1 mice	[57]
T_2*, Gd-DTPA-K6Aβ1-30	APP/PS1, APPswe mice	[46]
T_1w, Cyanine-Gd(III) complex	5×FAD mice	[47]
T_2*w GE Gd, Gd-DOTA, DOTAREM®,	APP_{SL}/$PS1_{M146L}$, $APP/PS1_{dE9}$, APP23, APP_{SwDI}, 3×Tg mice, PS1 mice	[44,55]
T_2*w GE, T_2w SE, Gd-pF(ab')24.1	APP/PS1 mice	[49]
T_2*w, Gd-DTPA-Aβ1-40, MION	APP/PS1 mice	[45]

SWI MGE RARE, APP-SiMag	3×Tg mice	[51]
T_2*w, USPIO-PEG-Aβ1-42.B	APP/PS1 mice	[50]
T_1w SE, ADx-001	APP/PS1 mice	[48]
T_2*w, anti-AβPP SPIONs	APP/PS1 mice	[52],
T_2*w, IgG4.1 NP	APPswe mice	[54]
T_2*w GE, SPIO	APP23, APP23×PS45 mice	[53]
T_1w, HMON-Aβ40	APP/PS1 mice	[37]
T_2*w MGE, $MnCl_2$	5×FAD mice, TgF344 rats	[56]
T_2*w, Cur-MNPs	5×FAD, APPswe mice	[67,68] #
T_2*w, W20/XD4-SPIONs	APP/PS1 mice	[66] #
T_2*w, NU4MNS Aβ oligomer	5×FAD mice	[63] #
T_2*, ACU193-MNS	Rabbit	[64] #

#Oligomer targeted; BSA, bovine serum albumin; CE, contrast enhanced; CESL, chemical exchange-sensitive spin-lock; CRAZED, COSY revamped with asymmetric z-GRE detection; Gd, gadolinium; GE, gradient echo; GRE, gradient recalled echo; MGE, multi-echo GRE; MION, monocrystalline iron oxide nanoparticles; $MnCl_2$, magnesium chloride; MNP, magnetic nanoparticle; MNS, magnetic nanostructures; MTC, Magnetization transfer contrast imaging; NP, nanoparticle; PEG, polyethylene glycol; QSM, quantitative susceptibility mapping; RARE, rapid acquisition with relaxation enhancement; SE, spin echo; SWI, susceptibility weighted imaging; USPION, Ultrasmall superparamagnetic iron oxide nanoparticles; w, weighted;

Preprints (www.preprints.org) | NOT PEER-REVIEWED | Posted: 15 October 2021 doi:10.20944/preprints202110.0231.v1

Table 2 MRI for functional and neurochemical changes in animal models of amyloidosis

MRI	Animal	References
rsfMRI BOLD	$APP^{NL-F/NL-F}$ ki mice	[92,98]
	APP/PS1 mice	[94,95,100,119,230]
	arcAβ mice	[90,94,146]
	TgCRND8 mice	[193].
	TgF344-AD rats	[102,231]
	PDAPP mice	[91]
	APPswe mice	[91,128]
	McGill-R-Thy1-APP rats	[232]
	3×Tg mice	[93]
	E22ΔAβ mice	[94]
	TetO-APPswe/ind mice	[99]
ASL	Bigenic mice	[120],
	arcAβ mice	[107,108]
	3×Tg mice	[233]
	APP DSL ki mice	[234],
	APP23 mice	[33,235]
	APP/PS1 mice	[104,105,119,123,235-239]
	J20 mice	[109]
	Tg-SwDI mice	[240,241]
	PS2APP mice	[111]
	5×FAD mice	[135,242]
	TetOAPPswe, CAA mice	[243]
	APPswe mice	[110,244]
fMRI CBV	BiAT mice	[120,245]
	APP23 mice	[53,115,118,153,246]
	arcAβ mice	[114] [107]
	PDAPP mice	[247]
	APP/PS1 mice	[119,238]

Preprints (www.preprints.org) | NOT PEER-REVIEWED | Posted: 15 October 2021 doi:10.20944/preprints202110.0231.v1

	APPswe mice	[230]
	J20 mice	[248]
MEMRI	3×Tg mice	[85]
	APP/PS1-Ki mice	[78]
	J20 mice	[79]
	APPswe mice	[35,83,84,110]
	5×FAD mice	[56,80]
	CVN-AD mice	[81]
	TgF344 rats	[56]
^{17}OZTE $CMRO_2$	APPPS1 mice	[249]
DSC	5×FAD, APOE mice	[202]
DGE	APP/PS1 mice	[134]
CEST	APP23 mice	[133]
	APP/PS1 mice	[136,137].
	5×FAD mice	[135]
MRS	TgF344 rats	[132]
	J20 mice	[109]
	APP/PS1 mice	[121-126]
	5×FAD mice	[130]
	3×Tg mice	[129]
	APPswe mice	[127,128].
	TASTPM, APP/PS2/Tau mice	[131]

ASL, arterial spin labeling; BOLD, blood-oxygen-level-dependent; CBF, cerebral blood flow; CBV, cerebral blood volume; CE, contrast enhanced; CEST, chemical exchange saturation transfer; $CMRO_2$, cerebral metabolic rate of oxygen consumption; DCE, dynamic contrast-enhanced; DGE, dynamic glucose-enhanced; DSC, dynamic susceptibility contrast; fMRI, functional magnetic resonance imaging; MEMRI, magnesium enhanced magnetic resonance imaging; MRA, magnetic resonance angiography; MRS, magnetic resonance spectroscopy; ZTE, zero echo time;

 doi:10.20944/preprints202110.0231.v1

Preprints (www.preprints.org) | NOT PEER-REVIEWED | Posted: 15 October 2021 doi:10.20944/preprints202110.0231.v1

Table 3. MRI for detecting atrophy, white matter and cerebral vasculature alterations in animal models of amyloidosis

MRI	Animal	References
T_2	APP/J20 mice	[169]
	APP/PS2/Tau mice	[131]
	TASTPM mice	[131,167]
	APP/PS1 mice	[105,125,164,168,236]
	McGill-R-Thy1-APP rats	[162]
	PDAPP mice	[250,251]
	APP-Au mice	[252]
	3×Tg mice	[93,165,253]
	APPswe mice	[244]
	APP/PS1KI mice	[166]
	APP/TTA mice	[254]
DKI	APP/PS1 mice	[184]
	3×Tg mice	[188]
qMTI	APPswe mice	[178]
DTI	TgF344 rats	[183]
	APPswe mice	[175,178,186,255]
	PDAPP mice	[176]
	App^{NL-G-F} knock-in mice	[72]
	APP/PS1 mice	[123,171,179,187,189,256]
	APP23 mice	[191]
	3×Tg mice	[93,177,188,190,257,258]
	TgCRND8 mice	[193]
	APP/TTA mice	[81,254]
	CVN-AD mice	[97]
	5×FAD mice	[135]
SWI, QSM	arcAβ mice	[146,147,154]
	APP/PS1 mice	[148]

Preprints (www.preprints.org) | NOT PEER-REVIEWED | Posted: 15 October 2021 doi:10.20944/preprints202110.0231.v1

	CVN-AD mice	[81]
T_2*	Tg SwDI mice	[145]
T_2*w	APP23 mice	[144]
DCE	5×FAD, APOE mice	[202]
MFAME-DCE	TgF344 rats	[203,204]
T_2*w, MPIOs-αVCAM-1	APP/PS1 mice	[160]
QUTE-CE	APOE4 rats	[156]
DWI	5×FAD mice	[155]
	arcAβ mice	[147,149,152]
MRA	APP/PS1 mice	[112,259]
	APP23 mice	[118,153]
	APPswe mice	[260]
MION	5×FAD mice	[155]
	5×FAD mice	[157]
MRE	APP/PS mice	[159]
	APP23 mice	[158]

BBB, blood-brain barrier; CE, contrast enhanced; CV, cerebral viscoelastic; DCE, dynamic contrast-enhanced; DGE, dynamic glucose-enhanced; DKI, diffusional kurtosis imaging; DTI, diffusion tensor imaging; DWI, diffusion-weighted imaging; MFAME, multi-flip angle multi-echo; MION, monocrystalline iron oxide nanoparticle; MPIOs, micro-sized particles of iron oxide; VCAM-1, vascular cell adhesion molecule-1; MRA, magnetic resonance angiography; MRE, magnetic resonance elastography qMTI, quantitative magnetization transfer imaging; QSM, quantitative susceptibility mapping; QUTE-CE, quantitative ultrashort time-to-echo, contrast enhanced; SWI, susceptibility weighted imaging; w, weighted:

Preprints (www.preprints.org) | NOT PEER-REVIEWED | Posted: 15 October 2021 doi:10.20944/preprints202110.0231.v1

Figure legends

Figure 1 Functional MRI and amyloid imaging in amyloidosis animal models. (a-d) Aberrant functional connectivity (FC) in the default mode-like network (DMN) in the Tet-Off APP mice with doxycycline treatment. (a) difference in FC within (nodes) and between (lines) regions in the DMN over time, week 0, 8, 16, 24. The inter-node FC difference is represented by the lines, with the colour scale illustrating the actual FC difference between Tet-Off APP and Ctrl, with orange indicating a stronger connection in the TG mice. The intra-node size represents the difference of the average FC of a specific region with all other regions inside DMN. (**c**) ROI-based FC analysis. FC matrices show the average z-transformed functional connectivity (zFC) for Ctrl (supra-diagonal) and TG (sub-diagonal) animals at week 0, 8, 16 and 28 post doxycycline treatment. Each square indicates the zFC between a pair of ROIs. The colour scale represents the connectivity strength with white indicating a low zFC and red/blue indicating positive/ negative zFC values. (**d**) Average FC within each network. Mean FC (z-score) over time for both groups in the whole brain, the default-mode like network; dashed line corresponds to TG group and full line to the Ctrl group. *$p < 0.05$; ***$p < 0.001$. Reproduced from [99] with permission from Springer Nature. (**e**) MRI amyloid imaging. (A) T_2*-weighted image at 16.4 T of 30-mo-old transgenic APP23 mouse and (B) corresponding amyloid histology; (C) T_2*-weighted image at 16.4 T of control mouse. Mammillothalamic tract and perifornical nucleus (red arrowheads). (D) Higher magnification of A and B of single amyloid plaques (blue arrowheads). Reproduced from [33] with permission from Society of Nuclear Medicine and Molecular Imaging. (**f**) *In vivo* T1-weighted MR pseudocolor mapped images of 6-month-old double Tg-AD and age-matched wild-type mice before and after injection of Cyanine-Gd(III) complex via tail vein at different depths in which the images were taken every 10 μm apart after 90 min post-injection of the probe on a 7.0 T MR scanner. Reproduced from [47] with permission from American Chemical Society. (**g, h**) W20/XD4-SPIONs characterization (g). The carboxyl of PEG on the paramagnetic iron oxide nanoparticles (SPIONs) was activated with EDC and NHS. SR-A activator XD4 and oligomer-specific scFv antibody W20 were conjugated to the nanoparticles. (h) *In vivo* T_2*-weighted images of the probe distribution in AD mouse brains after intravenous injection of W20/XD4-SPIONs, W20-SPIONs and SPIONs. Boxed regions are shown at higher magnification or stained by the Prussian blue. Scale bar, 1 mm. Reproduced from [66] with permission from Dovepress.

Figure 2 MRI of Blood-brain barrier permeability and cerebrovasculature in amyloidosis animal models. (**a-d**) T_2-weighted scans displaying regions of interest: primary somatosensory

Preprints (www.preprints.org) | NOT PEER-REVIEWED | Posted: 15 October 2021 doi:10.20944/preprints202110.0231.v1

cortex (Ctx) and hippocampus (Hipp). b,c, Representative K^{trans} maps (b) and values (c) in the Ctx and Hipp in APOE3 (E3, blue empty circles), APOE4 (E4, blue-filled circles), APOE3; 5×FAD (E3+FAD, red empty circles) and APOE4;5×FAD (E4+FAD, red-filled circles) mice generated from dynamic contrast enhanced-MRI scans. (**d**) Fibrinogen+ perivascular capillary deposits (red) in the Ctx. Blue, lectin+ endothelial profiles; scale bar, 20 µm. Reproduced with permission from [202] from Springer Nature. (**e-h**) High-resolution magnetic resonance angiography (MRA). (e) Time-of-flight-MRA intra- and extracranial vasculature of 24-month-old wild-type and arcAβ mouse (A, B) in sagittal, axial, and horizontal views. flow voids are seen in extracranial vessels (white arrows). Sections of maximum intensity projections (MIPs) of the anterior cerebral artery of a 4- and a 24-month-old (C, D) wild-type control mouse. Scale bar, 1 mm. (**f**) Contrast-enhanced MRA; MIPs derived from a 3D stack of difference images viewed in horizontal (*A*), sagittal (*B–D*), and axial (*E*) orientation. (**g-h**) Semiautomated analysis of intracortical vessel density. (g) significant decrease in the number of vessels was observed in 24-month-old arcAβ compared with wild-type mice corresponding to 3, 6, and 9 pixels, (*p < 0.05, repeated-measures ANOVA and Tukey's test). (h) number of vessels categorized according to their estimated vessel radius when the connectivity threshold was set to 3. Reproduced with permission from [152] from Society of Neuroscience. (**i, j**) Regional hypoperfusion in aged arcAβ mice assessed by arterial spin labeling MRI. Anatomical position of perfusion MRI and T_2-weighted scan on the sagittal view of the anatomical reference image and representative regions of interest (cortex (red) and thalamus (blue)) Representative coronal cerebral blood flow (CBF) map of 6- and 24-months-old wild-type littermate; (j) Reduced CBF in the cortex of 24-months old arcAβ compared with age-matched wild-type mice and 6-months old arcAβ and; *$p < 0.05$, one-way ANOVA with *post hoc* correction. Reproduced from [108] with permission from Elsevier.

Preprints (www.preprints.org) | NOT PEER-REVIEWED | Posted: 15 October 2021 doi:10.20944/preprints202110.0231.v1

Fig. 1

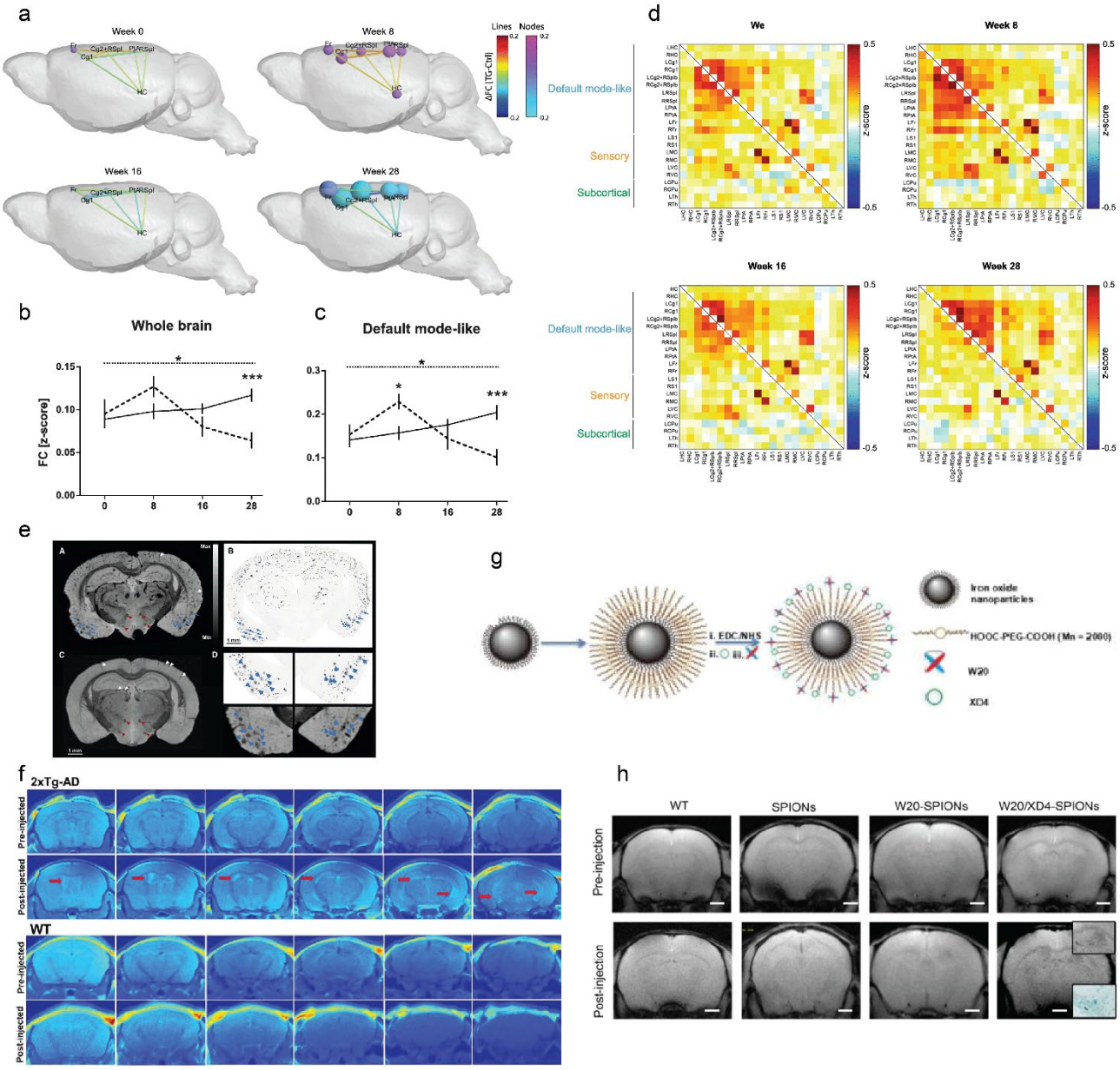

Preprints (www.preprints.org) | NOT PEER-REVIEWED | Posted: 15 October 2021 doi:10.20944/preprints202110.0231.v1

Fig. 2